Hindawi
Mathematical Problems in Engineering
Volume 2020, Article ID 3146762, 17 pages
https://doi.org/10.1155/2020/3146762

Research Article

Backstepping Sliding Mode Robust Control for a Wire-Driven Parallel Robot Based on a Nonlinear Disturbance Observer

Yuqi Wang,[1,2] **Qi Lin**,[2] **Lei Zhou**,[1] **Xinxin Shi**,[1] **and Lei Wang**[1]

[1]*School of Automation, Nanjing Institute of Technology, Nanjing, China*
[2]*Xiamen University, Xiamen, China*

Correspondence should be addressed to Yuqi Wang; 940898628@qq.com

Received 1 October 2019; Revised 11 January 2020; Accepted 27 January 2020; Published 24 March 2020

Academic Editor: Leonardo Acho

Based on a nonlinear disturbance observer, a backstepping sliding mode robust control is proposed for a wire-driven parallel robot (WDPR) system used in the wind tunnel test to dominate the motion of the end effector. The control method combines both the merits of backstepping control and sliding mode robust control. The WDPR is subject to different types of disturbances, and these disturbances will affect the motion precision of the end effector. To overcome these problems, a nonlinear disturbance observer (NDO) is designed to reject such disturbances. In this study, the design method of the nonlinear disturbance observer does not require the reliable dynamic model of the WDPR. Moreover, the design method can be used not only in the WDPR but also in other parallel robots. Then, a backstepping design method is adopted and a sliding mode term is introduced to construct a desired controller, and the disturbances are compensated in the controller to reduce the switching gain and guarantee the robustness. For the sake of verifying the stabilization of the closed-loop system, the Lyapunov function is constructed to analyze the stabilization of the system. Finally, the feasibility and validity of the proposed control scheme are proved through both simulation and experimental results.

1. Introduction

The wind tunnel test is a flight condition test, which simulates an aircraft in a real atmospheric environment. And it is the most important method to predict the aerodynamic performance of the aircraft. In the wind tunnel test, model support plays an extremely important effect in the study of aerodynamics and the development of new aircraft. The traditional rigid support mode, due to the support frame, causes distortion of the flow around the model, which makes the model test results different from the aerodynamic characteristics of the real aircraft. To improve the data accuracy of the wind tunnel test, the change of support mode of the wind tunnel model is one of the urgent problems to be solved.

In the last few years, wire (cable)-driven parallel robots have developed rapidly. Researchers have done a lot of research and analysis for wire (cable)-driven parallel robots. Chen et al. [1] designed a 7-DOF cable-driven humanoid arm and proposed the kinematic calibration issues in order to improve its motion control accuracy. Zi et al. [2] analyzed a cable parallel manipulator with and without hybrid-driven planar five-bar mechanism (HDPM). Yuan et al. [3] presented an original approach to analyze the modal interaction and illustrated this approach by numerical investigations and experimental analyses. Gao et al. [4] presented a novel bio-inspired cable-driven parallel robot with a flexible spine and investigated inverse kinematics and optimized the cable placements to minimize the actuating cable force. Aflakian et al. [5] presented an experimental study on the modeling and control for underconstrained cable-driven parallel robots (CDPRs). Heo et al. [6] improved the dynamic stability of CDPRs by means of frequency-based variable constraints over the whole workspace.

However, wire (cable)-driven parallel robots have multiple properties such as strong coupling, nonlinearity, and time variant [7]; these may cause difficulties in achieving accuracy control. For the sake of solving these problems,

various control methods have been developed rapidly. For the fully constrained cable-driven parallel robot, Khosravi and Taghirad [8] proposed a robust PID control. However, this method does not consider the external disturbance and the verification experiment is only for a planar CDPM. In 2015, Babaghasabha et al. [9] also presented an adaptive robust sliding mode controller for the fully constrained cable-driven parallel robot. Although the method had been verified in practice, it had increased the complexity of the system and the difficulty of physical realization. Kraus et al. [10] presented a position-force hybrid control. However, the actual trajectory performance is not good because the external disturbance is not considered. For a cable-driven parallel system, Wang et al. [11] studied the problem of type-2 fuzzy adaptive inverse control. However, due to the limitation of adaptive inverse control for the complex nonlinear system, interval type-2 fuzzy nonlinear models are considered, thus increasing the complexity of system control. For a fully constrained planar cable robot, Babaghasabha et al. [12] proposed an adaptive robust controller on the basis of the singular perturbation theory. However, the method was only verified by simulation on a planar cable-driven parallel robot. And there is no specific explanation and verification whether it can be used in space parallel robots. Jabbari Asl and Yoon et al. [13] also designed a robust tracking controller for fully constrained CDPRs. However, the error between the desired path and robot's trajectories in the X_aY_a plane is large according to the simulation results.

In the perspective of wind tunnel tests, some researchers have sensitively captured the advantages and application prospects of wire (cable)-driven parallel robots. Therefore, in recent years, they have proposed that wire (cable)-driven parallel robots can be introduced into the wind tunnel test, which provides a new method for the supporting technology of the aircraft model [14, 15]. However, as concluded from the previous studies, the above control methods cannot solve the control problem of WDPR in the wind tunnel test very well. Because during the operation of wire (cable)-driven parallel robots, external disturbances are usually unavoidable. To control the pose of the end-effector during the operation, this study proposes a backstepping sliding mode robust control based on a nonlinear disturbance observer, thus improving the robustness and accuracy of the control method. The main contribution of this study is that the backstepping sliding mode robust control method is applied to a 6-DOF 8-wire-driven parallel robot which has been developed by us and used in the wind tunnel test. And the advantages and significance of the proposed control method is that it can effectively deal with the nonlinearities, joint frictions, external disturbances, and dynamic uncertainties of the WDPR.

The rest of this study is organized as follows. In Section 2, the problem formulation is described. The designed nonlinear disturbance observer is presented in Section 3. Moreover, the design of backstepping sliding mode robust control and Lyapunov stability analysis are addressed in Section 4. In Sections 5 and 6, the simulation results and the prototype experimental results are given, respectively. Finally, the conclusion is drawn in Section 7.

2. Problem Formulation

In this section, we will give the composition, working principle, dynamic equations, properties on the WDPR, and an initial disturbance observer, which play a central effect in designing the nonlinear disturbance observer and the controller.

2.1. System Description. The WDPR and its wire structure are shown in Figure 1. In this study, the WDPR is designed for the low-speed wind tunnel test. It is a nonlinear parallel system with multiinput and multioutput (MIMO). And it suffers from different types of disturbances, for instance, frictions between the traction wires and pulleys, parameter uncertainties, unknown payloads, and unmodeled dynamics. The WDPR is composed of the end effector (standard dynamics model (SDM)), a drive system, a control system, a vision measurement system, frame, and so on. Through the pulley hinge point (B_i, $i = 1, 2, 3, \ldots, 8$), the connection point (P_i, $i = 1, 2, 3, \ldots, 8$) on the end-effector of the moving platform is connected with one end of the traction wire. Through controlling the length variation of eight wires, the end effector is made to do 6-DOF motion of 3 positions and 3 attitude angles in space. The structure schematic diagram is shown in Figure 2.

The dynamic modeling of the WDPR is mainly composed of two parts: the dynamic modeling of the end effector and the dynamic modeling of the drive system. And the dynamic modeling of the end effector is the design foundation of motion control. The two dynamic equations are shown as follows:

$$\begin{cases} \mathbf{M}_0\ddot{\boldsymbol{\theta}}_m + \mathbf{C}_0\dot{\boldsymbol{\theta}}_m + \mu\mathbf{T} = \boldsymbol{\tau} + \boldsymbol{\tau}_1, \\ \mathbf{M}(\mathbf{X})\ddot{\mathbf{X}} + \mathbf{N}(\mathbf{X}, \dot{\mathbf{X}}) - \mathbf{w}_g - \mathbf{w}_e = -\mathbf{J}^{\mathrm{T}}\mathbf{T}, \end{cases} \tag{1}$$

where $\mathbf{M}_0$ is the inertia matrix equivalent to the driver, $\mathbf{C}_0$ is the viscous friction coefficient matrix equivalent to the driver, μ is the transmission coefficient of the ball screw, $\boldsymbol{\theta}_m \in R^{8\times1}$ is the motor angle vector, $\mathbf{T} \in R^{8\times1}$ is the wire tension vector, $\boldsymbol{\tau} \in R^{8\times1}$ is the output torque vector of the driver, $\boldsymbol{\tau}_1 \in R^{8\times1}$ is the vector of external disturbances, $\mathbf{M}(\mathbf{X}) \in R^{6\times6}$ is the inertial matrix of the end-effector, $\mathbf{X} = (X_P, Y_P, Z_P, \phi, \theta, \psi)^{\mathrm{T}}$ is the pose of the end-effector, $(X_P, Y_P, Z_P)^{\mathrm{T}}$ is the coordinate of point $\mathbf{P}$ relative to the static platform, $(\phi, \theta, \psi)^{\mathrm{T}}$ is the attitude angle of the end-effector, and ϕ, θ, and ψ are the roll angle, pitch angle, and yaw angle, respectively; $\dot{X} \in R^{6\times1}$ is the pose velocity of the end-effector, $\mathbf{J} \in R^{8\times6}$ is a Jacobi matrix, $\mathbf{N}(\mathbf{X}, \dot{X}) \in R^{6\times1}$ is a nonlinear coriolis centrifugal matrix, $\mathbf{w}_g \in R^{6\times1}$ is a gravitational vector of the end-effector, $\mathbf{w}_g = (0, 0, mg, 0, 0, 0)^{\mathrm{T}}$, and $\mathbf{w}_e \in R^{6\times1}$ is subject to external dynamic loads at the end-effector, and $\mathbf{w}_e = [\mathbf{f}_e; \boldsymbol{\tau}_e]$. $\mathbf{f}_e$ and $\boldsymbol{\tau}_e$ are the aerodynamic and dynamic moments acting on the end-effector, respectively. If the dynamic analysis is carried out under the condition of 0 wind speed, then $\mathbf{w}_e = 0$:

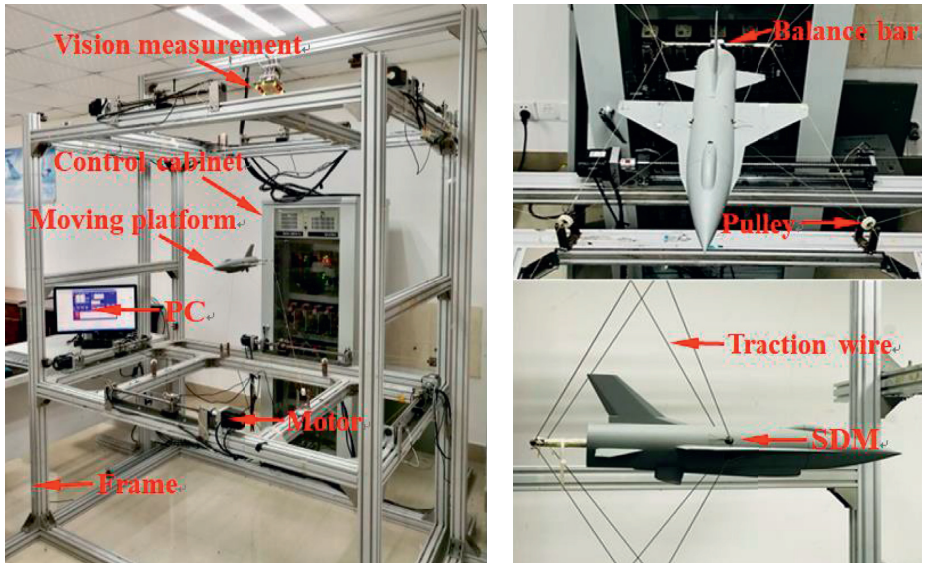

(a) (b)

Figure 1: WDPR and its wire structure.

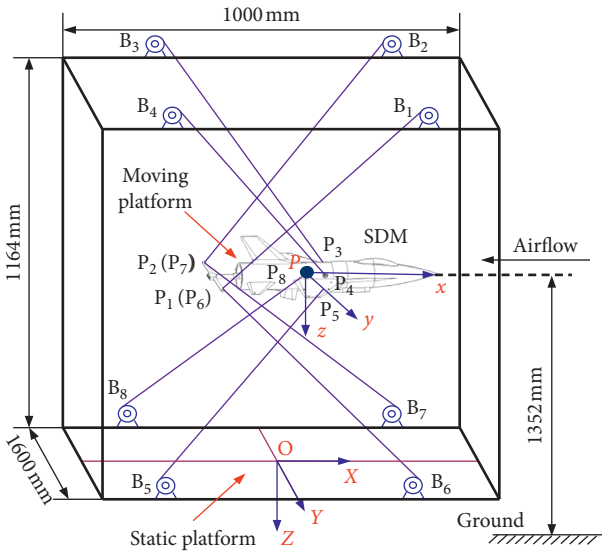

Figure 2: Structure schematic diagram of the WDPR.

$$\mathbf{M}(\mathbf{X}) = \begin{bmatrix} (m\mathbf{I})_{3\times3} & \mathbf{0}_{3\times3} \\ \mathbf{0}_{3\times3} & \mathbf{A}_G\mathbf{H} \end{bmatrix},$$
$$\mathbf{N}(\mathbf{X}, \dot{X}) = \begin{bmatrix} \mathbf{0}_{3\times1} \\ \mathbf{A}_G\dot{\mathbf{H}}\dot{\mathbf{Q}} + (\mathbf{H}\dot{\mathbf{Q}}) \times \left(\mathbf{A}_G\mathbf{H}\dot{\mathbf{Q}}\right) \end{bmatrix}_{6\times1},$$
$$\mathbf{H} = \begin{bmatrix} \cos\theta & \cos\psi & -\sin\psi & 0 \\ \cos\theta & \sin\psi & \cos\psi & 0 \\ -\sin\theta & 0 & 1 & \end{bmatrix}, \quad (2)$$
$$\dot{Q} = \begin{bmatrix} \dot{\phi} \\ \dot{\theta} \\ \dot{\psi} \end{bmatrix}.$$

Here, $\mathbf{A}_G$ is the inertia matrix of the end-effector, and $\dot{Q}$ is the attitude angular velocity vector.

The relationship between the pose velocity $\dot{X}$, the wire length $\mathbf{L}$, and the motor angle $\boldsymbol{\theta}_m$ is denoted by the following equations:

$$\dot{\mathbf{L}} = \mu \cdot \dot{\boldsymbol{\theta}}_{\mathrm{m}} = \mathbf{J}\mathbf{G}\dot{X}, \quad (3)$$

$$\ddot{\mathbf{L}} = \mu \cdot \ddot{\boldsymbol{\theta}}_m = \dot{\mathbf{J}}\mathbf{G}\dot{X} + \mathbf{J}\dot{G}\dot{X} + \mathbf{J}\mathbf{G}\ddot{X}, \quad (4)$$

where $\mathbf{G} \in R^{6\times6}$ is a transition matrix based on the attitude angle, $\mathbf{G} = \begin{bmatrix} \mathbf{I}_{3\times3} & 0_{3\times3} \\ 0_{3\times3} & \mathbf{H} \end{bmatrix}$.

According to equations (1), (3), and (4), we obtain the whole dynamic equation of the WDPR with 6 DOF:

$$\left(\mathbf{M}(\mathbf{X}) - \frac{1}{\mu^2} \cdot \mathbf{J}^{\mathrm{T}}\mathbf{M}_0\mathbf{J}\mathbf{G}\right)\ddot{X} - \frac{1}{\mu^2}\left(\mathbf{J}^{\mathrm{T}}\mathbf{M}_0\dot{J}\mathbf{G} + \mathbf{J}^{\mathrm{T}}\mathbf{M}_0\mathbf{J}\dot{G} + \mathbf{J}^{\mathrm{T}}\mathbf{C}_0\mathbf{J}\mathbf{G}\right)\dot{X}$$
$$= -\frac{1}{\mu} \cdot \mathbf{J}^{\mathrm{T}}\left(\boldsymbol{\tau} + \boldsymbol{\tau}_1\right) + \mathbf{w}_g + \mathbf{w}_e - \mathbf{N}(\mathbf{X}, \dot{X}). \quad (5)$$

Equation (5) is simplified as the following equation:

$$-\mu\left(\mathbf{M}(\mathbf{X}) - \frac{1}{\mu^2} \cdot \mathbf{J}^{\mathrm{T}}\mathbf{M}_0\mathbf{J}\mathbf{G}\right)\ddot{X} + \frac{1}{\mu}\left(\mathbf{J}^{\mathrm{T}}\mathbf{M}_0\dot{J}\mathbf{G} + \mathbf{J}^{\mathrm{T}}\mathbf{M}_0\mathbf{J}\dot{G} + \mathbf{J}^{\mathrm{T}}\mathbf{C}_0\mathbf{J}\mathbf{G}\right)$$
$$\dot{X} + \mu\mathbf{w}_g = \mathbf{J}^{\mathrm{T}}\boldsymbol{\tau} + \boldsymbol{\tau}_d, \quad (6)$$

where $\boldsymbol{\tau}_d = \mathbf{J}^{\mathrm{T}}\boldsymbol{\tau}_1 + \mu\mathbf{N}(\mathbf{X}, \dot{X}) - \mu\mathbf{w}_e$.

Let

$$\mathbf{A}(\mathbf{X}) = -\mu\left(\mathbf{M}(\mathbf{X}) - \frac{1}{\mu^2} \cdot \mathbf{J}^{\mathrm{T}}\mathbf{M}_0\mathbf{J}\mathbf{G}\right),$$
$$\mathbf{B}(\mathbf{X}) = \frac{1}{\mu}\left(\mathbf{J}^{\mathrm{T}}\mathbf{M}_0\dot{J}\mathbf{G} + \mathbf{J}^{\mathrm{T}}\mathbf{M}_0\mathbf{J}\dot{G} + \mathbf{J}^{\mathrm{T}}\mathbf{C}_0\mathbf{J}\mathbf{G}\right). \quad (7)$$

Equation (6) is simplified as the following equation:

$$\mathbf{A}(\mathbf{X})\ddot{X} + \mathbf{B}(\mathbf{X})\dot{X} + \mu\mathbf{w}_g = \mathbf{J}^{\mathrm{T}}\boldsymbol{\tau} + \boldsymbol{\tau}_d. \tag{8}$$

The WDPR has several properties. In this study, these properties will be used when designing the nonlinear disturbance observer and the controller. These properties are listed as follows.

Property 1. The inertial matrix $\mathbf{M}(\mathbf{X})$ of the end-effector is symmetric and positive definite. And its norm is bounded:

$$\begin{aligned} \mathbf{M}^{-1}(\mathbf{X}) &= \mathbf{M}^{-\mathrm{T}}(\mathbf{X}) > 0, \\ \mathbf{M}(\mathbf{X}) &= \mathbf{M}^{\mathrm{T}}(\mathbf{X}) > 0, \end{aligned} \tag{9}$$

$\mathbf{M}_0$ and $\mathbf{G}$ are symmetric and positive definite; therefore,

$$-\mu\left(\mathbf{M}(\mathbf{X}) - \frac{1}{\mu^2}\cdot\mathbf{J}^{\mathrm{T}}\mathbf{M}_0\mathbf{J}\mathbf{G}\right) = \left(-\mu\left(\mathbf{M}(\mathbf{X}) - \frac{1}{\mu^2}\cdot\mathbf{J}^{\mathrm{T}}\mathbf{M}_0\mathbf{J}\mathbf{G}\right)\right)^{\mathrm{T}}, \tag{10}$$

that is,

$$\begin{aligned} \mathbf{A}^{-1}(\mathbf{X}) &= \mathbf{A}^{-\mathrm{T}}(\mathbf{X}) > 0, \\ \mathbf{A}(\mathbf{X}) &= \mathbf{A}(\mathbf{X})^{\mathrm{T}} > 0. \end{aligned} \tag{11}$$

In the same way, $\mathbf{B}(\mathbf{X})$ and $\mathbf{B}^{-1}(\mathbf{X})$ are symmetric and positive definite by verification.

Property 2. The Jacobi matrix $\mathbf{J}$ meets the following properties:

$$\begin{aligned} \mathbf{J}^{\mathrm{T}}\left(\mathbf{J}^{\mathrm{T}}\right)^{+} &= \mathbf{I}_{6\times 6}, \\ (\mathbf{J})^{+}\mathbf{J} &= \mathbf{I}_{6\times 6}. \end{aligned} \tag{12}$$

Property 3. The transition matrix $\mathbf{G}$ meets the following properties:

$$\begin{aligned} \mathbf{G}\mathbf{G}^{-1} &= \mathbf{I}_{6\times 6}, \\ \mathbf{G}^{-1}\mathbf{G} &= \mathbf{I}_{6\times 6}. \end{aligned} \tag{13}$$

where $\mathbf{I}_{6\times 6}$ is the identity matrix.

In practical engineering application, it is difficult to acquire complete information of the WDPR because of parameter uncertainties and external disturbances. Therefore, assume that the whole dynamic equation of the WDPR is as follows:

$$(\mathbf{A}(\mathbf{X}) + \Delta\mathbf{A}(\mathbf{X}))\ddot{X} + (\mathbf{B}(\mathbf{X}) + \Delta\mathbf{B}(\mathbf{X}))\dot{X} + \mu\mathbf{w}_g = \mathbf{J}^{\mathrm{T}}\boldsymbol{\tau} + \boldsymbol{\tau}_d, \tag{14}$$

where $\Delta\mathbf{A}(\mathbf{X})$ and $\Delta\mathbf{B}(\mathbf{X})$ are parameter uncertainties present in nonlinear systems.

Then, the total disturbance vector is defined as

$$\mathbf{D}(\mathbf{X}, \dot{X}, \ddot{X}) = \boldsymbol{\tau}_d - \Delta\mathbf{A}(\mathbf{X})\ddot{X} - \Delta\mathbf{B}(\mathbf{X})\dot{X}. \tag{15}$$

According to the above definition, the effects of all dynamic uncertainties, external disturbances, and joint frictions are concentrated in a single disturbance vector $\mathbf{D}(\mathbf{X}, \dot{X}, \ddot{X})$. It is seen from equation (8) that

$$\mathbf{A}(\mathbf{X})\ddot{X} + \mathbf{B}(\mathbf{X})\dot{X} + \mu\mathbf{w}_g = \mathbf{J}^{\mathrm{T}}\boldsymbol{\tau} + \mathbf{D}(\mathbf{X}, \dot{X}, \ddot{X}). \tag{16}$$

2.2. Initial Disturbance Observer. Since the total disturbance $\mathbf{D}(\mathbf{X}, \dot{X}, \ddot{X})$ will adversely affect the precision of the end-effector of the WDPR, a disturbance observer is an ordinary means and can be used to reject these disturbances. A disturbance observer equates the difference between the actual object and the nominal model caused by the external disturbance and the change of model parameters to control input, that is, the equivalent disturbance is observed, and the equivalent compensation is introduced into control to realize the complete control of the disturbance. A basic idea of designing the observer is to modify the estimation by the difference between estimated output and actual output. Hence, equation (16) can be written as

$$\mathbf{D}(\mathbf{X}, \dot{X}, \ddot{X}) = \mathbf{A}(\mathbf{X})\ddot{X} + \mathbf{B}(\mathbf{X})\dot{X} + \mu\mathbf{w}_g - \mathbf{J}^{\mathrm{T}}\boldsymbol{\tau}. \tag{17}$$

Therefore, according to the dynamic model of equation (17), the initial disturbance observer can be designed as follows:

$$\begin{aligned} \dot{\hat{\mathbf{D}}}(\mathbf{X}, \dot{X}, \ddot{X}) &= \mathbf{K}(\mathbf{X})\left(\mathbf{D}(\mathbf{X}, \dot{X}, \ddot{X}) - \hat{D}(\mathbf{X}, \dot{X}, \ddot{X})\right) \\ &= -\mathbf{K}(\mathbf{X})\hat{D}(\mathbf{X}, \dot{X}, \ddot{X}) + \mathbf{K}(\mathbf{X})\mathbf{D}(\mathbf{X}, \dot{X}, \ddot{X}) \\ &= -\mathbf{K}(\mathbf{X})\hat{D}(\mathbf{X}, \dot{X}, \ddot{X}) + \mathbf{K}(\mathbf{X})\Big(\mathbf{A}(\mathbf{X})\ddot{X} + \mathbf{B}(\mathbf{X}) \\ &\quad \cdot \dot{X} + \mu\mathbf{w}_{\mathrm{g}} - \mathbf{J}^{T}\boldsymbol{\tau}\Big), \end{aligned} \tag{18}$$

where $\mathbf{K}(\mathbf{X})$ is the gain matrix of the observer and $\hat{D}(\mathbf{X}, \dot{X}, \ddot{X})$ is the estimated value of $\mathbf{D}(\mathbf{X}, \dot{X}, \ddot{X})$.

In general, there is no prior information about the derivative of the disturbance $\mathbf{D}(\mathbf{X}, \dot{X}, \ddot{X})$; therefore, it is assumed that the variation of the disturbance is slow relative to the dynamic characteristics of the observer, that is, $\dot{\mathbf{D}}(\mathbf{X}, \dot{X}, \ddot{X}) = 0$. Then, let the estimation error of the nonlinear disturbance observer be

$$\tilde{\mathbf{D}}(\mathbf{X}, \dot{X}, \ddot{X}) = \mathbf{D}(\mathbf{X}, \dot{X}, \ddot{X}) - \hat{D}(\mathbf{X}, \dot{X}, \ddot{X}). \tag{19}$$

Combining equation (19) with the initial disturbance observer (18) yields

$$\begin{aligned} \dot{\tilde{\mathbf{D}}}(\mathbf{X}, \dot{X}, \ddot{X}) &= \dot{D}(\mathbf{X}, \dot{X}, \ddot{X}) - \dot{\hat{D}}(\mathbf{X}, \dot{X}, \ddot{X}) = \dot{\hat{D}}(\mathbf{X}, \dot{X}, \ddot{X}) \\ &= -\mathbf{K}(\mathbf{X})\left(\mathbf{D}(\mathbf{X}, \dot{X}, \ddot{X}) - \hat{D}(\mathbf{X}, \dot{X}, \ddot{X})\right) \\ &= -\mathbf{K}(\mathbf{X})\tilde{D}(\mathbf{X}, \dot{X}, \ddot{X}). \end{aligned} \tag{20}$$

That is, the observation error satisfies the constraint conditions:

$$\dot{\tilde{D}}(\mathbf{X}, \dot{X}, \ddot{X}) + \mathbf{K}(\mathbf{X})\tilde{D}(\mathbf{X}, \dot{X}, \ddot{X}) = 0. \tag{21}$$

3. Nonlinear Disturbance Observer Design

Due to the uncertainties of the WDPR and external disturbance (the total disturbance), for the sake of reducing the

impact of the total disturbance on the WDPR and improving the control precision of the system, a nonlinear disturbance observer (NDO) is designed to approach the system disturbance. Based on the advantages of references [16, 17], first, the auxiliary variable is designed as follows:

$$\mathbf{z} = \hat{D}(\mathbf{X}, \dot{X}, \ddot{X}) - \mathbf{Q}(\mathbf{X}, \dot{X}), \tag{22}$$

where $\mathbf{z} \in R^{6\times 1}$ and $\mathbf{Q}(\mathbf{X}, \dot{X})$ is a function vector.

Let

$$\dot{Q}(\mathbf{X}, \dot{X}) = \mathbf{K}(\mathbf{X})\mathbf{A}(\mathbf{X})\ddot{X}. \tag{23}$$

Then,

$$\begin{aligned}
\dot{\mathbf{z}} &= \dot{\hat{D}}(\mathbf{X}, \dot{X}, \ddot{X}) - \dot{Q}(\mathbf{X}, \dot{X}) = \dot{\hat{D}}(\mathbf{X}, \dot{X}, \ddot{X}) \\
&\quad - \mathbf{K}(\mathbf{X})\mathbf{A}(\mathbf{X})\ddot{X}, \\
\dot{\hat{D}}(\mathbf{X}, \dot{X}, \ddot{X}) &= -\mathbf{K}(\mathbf{X})\hat{D}(\mathbf{X}, \dot{X}, \ddot{X}) + \mathbf{K}(\mathbf{X})\left(\mathbf{A}(\mathbf{X})\ddot{X}\right. \\
&\quad \left. + \mathbf{B}(\mathbf{X})\dot{X} + \mu\mathbf{w}_g - \mathbf{J}^T\boldsymbol{\tau}\right), \\
\dot{z} &= \dot{\hat{D}}(\mathbf{X}, \dot{X}, \ddot{X}) - \dot{Q}(\mathbf{X}, \dot{X}) = \mathbf{K}(\mathbf{X})\left(\mathbf{A}(\mathbf{X})\ddot{X}\right. \\
&\quad \left. + \mathbf{B}(\mathbf{X})\dot{X} + \mu\mathbf{w}_g - \mathbf{J}^T\boldsymbol{\tau}\right) \\
&\quad - \mathbf{K}(\mathbf{X})\hat{D}(\mathbf{X}, \dot{X}, \ddot{X}) - \mathbf{K}(\mathbf{X})\mathbf{A}(\mathbf{X})\ddot{X}, \\
&= \mathbf{K}(\mathbf{X})\mathbf{A}(\mathbf{X})\ddot{X} + \mathbf{K}(\mathbf{X})\mathbf{B}(\mathbf{X})\dot{X} + \mathbf{K}(\mathbf{X})\mu\mathbf{w}_g \\
&\quad - \mathbf{K}(\mathbf{X})\mathbf{J}^T\boldsymbol{\tau} - \mathbf{K}(\mathbf{X})\hat{D}(\mathbf{X}, \dot{X}, \ddot{X}) - \mathbf{K}(\mathbf{X})\mathbf{A}(\mathbf{X})\ddot{X}, \\
&= \mathbf{K}(\mathbf{X})\mathbf{B}(\mathbf{X})\dot{X} + \mathbf{K}(\mathbf{X})\mu\mathbf{w}_g - \mathbf{K}(\mathbf{X})\mathbf{J}^T\boldsymbol{\tau} \\
&\quad - \mathbf{K}(\mathbf{X})\hat{D}(\mathbf{X}, \dot{X}, \ddot{X}).
\end{aligned} \tag{24}$$

The design nonlinear disturbance observer is as follows:

$$\begin{cases}
\dot{z} = \mathbf{K}(\mathbf{X})\mathbf{B}(\mathbf{X})\dot{X} + \mathbf{K}(\mathbf{X})\mu\mathbf{w}_g - \mathbf{K}(\mathbf{X})\mathbf{J}^T\boldsymbol{\tau} - \mathbf{K}(\mathbf{X})\hat{D}(\mathbf{X}, \dot{X}, \ddot{X}), \\
\hat{D}(\mathbf{X}, \dot{X}, \ddot{X}) = \mathbf{z} + \mathbf{Q}(\mathbf{X}, \dot{X}).
\end{cases} \tag{25}$$

Then,

$$\begin{aligned}
\dot{z} &= \mathbf{K}(\mathbf{X})\mathbf{B}(\mathbf{X})\dot{X} + \mathbf{K}(\mathbf{X})\mu\mathbf{w}_g - \mathbf{K}(\mathbf{X})\mathbf{J}^T\boldsymbol{\tau} - \mathbf{K}(\mathbf{X})(\mathbf{z} + \mathbf{Q}(\mathbf{X}, \dot{X})) \\
&= \mathbf{K}(\mathbf{X})\mathbf{B}(\mathbf{X})\dot{X} + \mathbf{K}(\mathbf{X})\mu\mathbf{w}_g - \mathbf{K}(\mathbf{X})\mathbf{J}^T\boldsymbol{\tau} - \mathbf{K}(\mathbf{X})\mathbf{z} \\
&\quad - \mathbf{K}(\mathbf{X})\mathbf{Q}(\mathbf{X}, \dot{X}), \\
&= \mathbf{K}(\mathbf{X})\left(\mathbf{B}(\mathbf{X})\dot{X} + \mu\mathbf{w}_g - \mathbf{J}^T\boldsymbol{\tau} - \mathbf{Q}(\mathbf{X}, \dot{X})\right) - \mathbf{K}(\mathbf{X})\mathbf{z}.
\end{aligned} \tag{26}$$

According to the above analysis, since $\dot{\tilde{D}}(\mathbf{X}, \dot{X}, \ddot{X}) = \dot{D}(\mathbf{X}, \dot{X}, \ddot{X}) - \dot{\hat{D}}(\mathbf{X}, \dot{X}, \ddot{X}) = -\dot{\hat{D}}(\mathbf{X}, \dot{X}, \ddot{X})$, $\dot{D}(\mathbf{X}, \dot{X}, \ddot{X}) = 0$, there are

$$\dot{\hat{D}}(\mathbf{X}, \dot{X}, \ddot{X}) = -\dot{z} - \dot{Q}(\mathbf{X}, \dot{X}). \tag{27}$$

Equations (23) and (25) are substituted into equation (27) and we obtain

$$\begin{aligned}
\dot{\hat{D}}(\mathbf{X}, \dot{X}, \ddot{X}) &= -\dot{z} - \dot{Q}(\mathbf{X}, \dot{X}) \\
&= -\mathbf{K}(\mathbf{X})\left(\mathbf{B}(\mathbf{X})\dot{X} + \mu\mathbf{w}_g - \mathbf{J}^T\boldsymbol{\tau} - \mathbf{Q}(\mathbf{X}, \dot{X})\right) \\
&\quad + \mathbf{K}(\mathbf{X})\mathbf{z} - \mathbf{K}(\mathbf{X})\mathbf{A}(\mathbf{X})\ddot{X}, \\
&= \mathbf{K}(\mathbf{X})(\mathbf{z} + \mathbf{Q}(\mathbf{X}, \dot{X})) - \mathbf{K}(\mathbf{X})\left(\mathbf{A}(\mathbf{X})\ddot{X}\right. \\
&\quad \left. + \mathbf{B}(\mathbf{X})\dot{X} + \mu\mathbf{w}_g - \mathbf{J}^T\boldsymbol{\tau}\right).
\end{aligned} \tag{28}$$

Let function vector $\mathbf{Q}(\mathbf{X}, \dot{X}) = \mathbf{P}\dot{X}$ and design the gain matrix $\mathbf{K}(\mathbf{X}) = \mathbf{P}\mathbf{A}^{-1}(\mathbf{X})$, where $\mathbf{P}$ is an invertible matrix; then, the observation error equation is as follows:

$$\dot{\tilde{D}}(\mathbf{X}, \dot{X}, \ddot{X}) + \mathbf{P}\mathbf{A}^{-1}(\mathbf{X})\tilde{D}(\mathbf{X}, \dot{X}, \ddot{X}) = 0, \tag{29}$$

where $\mathbf{P}$ is obtained through Linear Matrix Inequality (LMI), so that the gain matrix $\mathbf{K}(\mathbf{X})$ is obtained and the estimated value $\hat{D}(\mathbf{X}, \dot{X}, \ddot{X})$ approximates the disturbance by exponent.

Proof. For the sake of verifying whether the design nonlinear disturbance observer is convergent, a Lyapunov function is designed as follows:

$$V_0 = \tilde{D}^{\mathrm{T}}(\mathbf{X}, \dot{X}, \ddot{X})\mathbf{P}^{-\mathrm{T}}\mathbf{A}(\mathbf{X})\mathbf{P}^{-1}\tilde{D}(\mathbf{X}, \dot{X}, \ddot{X}). \tag{30}$$

□

Since $\mathbf{A}(\mathbf{X})$ is a symmetric and positive definite matrix, and the matrix $\mathbf{P}$ is invertible, the matrix $\mathbf{P}^{-\mathrm{T}}\mathbf{A}(\mathbf{X})\mathbf{P}^{-1}$ is also positive definite. Thus, the Lyapunov function V_0 is positive definite.

The Lyapunov function derivation is obtained with respect to time t, which is shown below:

$$\begin{aligned}
\dot{V}_0 &= \dot{\tilde{D}}^{\mathrm{T}}(\mathbf{X}, \dot{X}, \ddot{X})\mathbf{P}^{-\mathrm{T}}\mathbf{A}(\mathbf{X})\mathbf{P}^{-1}\tilde{D}(\mathbf{X}, \dot{X}, \ddot{X}) \\
&\quad + \tilde{D}^{\mathrm{T}}(\mathbf{X}, \dot{X}, \ddot{X})\mathbf{P}^{-\mathrm{T}}\dot{\mathbf{A}}(\mathbf{X})\mathbf{P}^{-1}\tilde{D}(\mathbf{X}, \dot{X}, \ddot{X}) \\
&\quad + \tilde{D}^{\mathrm{T}}(\mathbf{X}, \dot{X}, \ddot{X})\mathbf{P}^{-\mathrm{T}}\mathbf{A}(\mathbf{X})\mathbf{P}^{-1}\dot{\tilde{D}}(\mathbf{X}, \dot{X}, \ddot{X}).
\end{aligned} \tag{31}$$

From the error equation of the observer, we obtain

$$\begin{aligned}
\dot{\tilde{D}}^{\mathrm{T}}(\mathbf{X}, \dot{X}, \ddot{X}) &= -(\mathbf{K}(\mathbf{X})\tilde{D}(\mathbf{X}, \dot{X}, \ddot{X}))^{\mathrm{T}} \\
&= -\left(\mathbf{P}\mathbf{A}^{-1}(\mathbf{X})\tilde{D}(\mathbf{X}, \dot{X}, \ddot{X})\right)^{\mathrm{T}} \\
&= -\tilde{D}^{\mathrm{T}}(\mathbf{X}, \dot{X}, \ddot{X})\mathbf{A}^{-\mathrm{T}}(\mathbf{X})\mathbf{P}^{\mathrm{T}}.
\end{aligned} \tag{32}$$

Hence, the following can be obtained:

$$\begin{aligned}\dot{\mathbf{V}}_0 &= -\tilde{D}^{\mathrm{T}}(\mathbf{X},\dot{X},\ddot{X})\mathbf{A}^{-\mathrm{T}}(\mathbf{X})\mathbf{P}^{\mathrm{T}}\mathbf{P}^{-\mathrm{T}}\mathbf{A}(\mathbf{X})\mathbf{P}^{-1}\tilde{D}(\mathbf{X},\dot{X},\ddot{X})\\ &\quad+\tilde{D}^{\mathrm{T}}(\mathbf{X},\dot{X},\ddot{X})\mathbf{P}^{-\mathrm{T}}\dot{\mathbf{A}}(\mathbf{X})\mathbf{P}^{-1}\tilde{D}(\mathbf{X},\dot{X},\ddot{X})\\ &\quad+\tilde{D}^{\mathrm{T}}(\mathbf{X},\dot{X},\ddot{X})\mathbf{P}^{-\mathrm{T}}\mathbf{A}(\mathbf{X})\mathbf{P}^{-1}\dot{\tilde{D}}(\mathbf{X},\dot{X},\ddot{X})\\ &= -\tilde{D}^{\mathrm{T}}(\mathbf{X},\dot{X},\ddot{X})\mathbf{P}^{-1}\tilde{D}(\mathbf{X},\dot{X},\ddot{X})+\tilde{D}^{\mathrm{T}}(\mathbf{X},\dot{X},\ddot{X})\mathbf{P}^{-\mathrm{T}}\dot{\mathbf{A}}\\ &\quad\cdot(\mathbf{X})\mathbf{P}^{-1}\tilde{D}(\mathbf{X},\dot{X},\ddot{X})-\tilde{D}^{\mathrm{T}}(\mathbf{X},\dot{X},\ddot{X})\mathbf{P}^{-\mathrm{T}}\mathbf{A}(\mathbf{X})\mathbf{P}^{-1}\\ &\quad\cdot\mathbf{P}\mathbf{A}^{-1}(\mathbf{X})\tilde{D}(\mathbf{X},\dot{X},\ddot{X})\\ &= -\tilde{D}^{\mathrm{T}}(\mathbf{X},\dot{X},\ddot{X})\mathbf{P}^{-1}\tilde{D}(\mathbf{X},\dot{X},\ddot{X})+\tilde{D}^{\mathrm{T}}(\mathbf{X},\dot{X},\ddot{X})\mathbf{P}^{-\mathrm{T}}\dot{\mathbf{A}}\\ &\quad\cdot(\mathbf{X})\mathbf{P}^{-1}\tilde{D}(\mathbf{X},\dot{X},\ddot{X})-\tilde{D}^{\mathrm{T}}(\mathbf{X},\dot{X},\ddot{X})\mathbf{P}^{-\mathrm{T}}\tilde{D}(\mathbf{X},\dot{X},\ddot{X})\\ &= -\tilde{D}^{\mathrm{T}}(\mathbf{X},\dot{X},\ddot{X})\left(\mathbf{P}^{-1}-\mathbf{P}^{-\mathrm{T}}\dot{\mathbf{A}}(\mathbf{X})\mathbf{P}^{-1}+\mathbf{P}^{-\mathrm{T}}\right)\tilde{D}(\mathbf{X},\dot{X},\ddot{X}).\end{aligned} \tag{33}$$

To make $\dot{V}_0<0$, $(\mathbf{P}^{-1}-\mathbf{P}^{-\mathrm{T}}\dot{\mathbf{A}}(\mathbf{X})\mathbf{P}^{-1}+\mathbf{P}^{-\mathrm{T}})$ needs to satisfy a positive definite condition. Let

$$\mathbf{P}^{-1}-\mathbf{P}^{-\mathrm{T}}\dot{\mathbf{A}}(\mathbf{X})\mathbf{P}^{-1}+\mathbf{P}^{-\mathrm{T}}\geq\Pi, \tag{34}$$

where $\Pi>0$ and Π is a symmetric positive definite matrix.

Then,

$$\dot{V}_0\leq-\tilde{D}^{\mathrm{T}}(\mathbf{X},\dot{X},\ddot{X})\Pi\tilde{D}(\mathbf{X},\dot{X},\ddot{X}). \tag{35}$$

There is $\Pi'>0$ that makes $\dot{V}_0\leq-\tilde{D}^{\mathrm{T}}(\mathbf{X},\dot{X},\ddot{X})\Pi\tilde{D}(\mathbf{X},\dot{X},\ddot{X})=-\Pi'\mathbf{V}_0$.

From equation (34), the nonlinear disturbance observer exponentially converges, and the convergence accuracy depends on the value of parameter Π. The larger the value Π is, the faster the convergence rate is and the higher the precision is.

The design of the nonlinear disturbance observer can ultimately be attributed to solving the value of the invertible matrix $\mathbf{P}$. It is known that the value of $\mathbf{P}$ can be obtained by using Linear Matrix Inequality (LMI).

Therefore, let $\mathbf{Z}=\mathbf{P}$, $\mathbf{Z}^{\mathrm{T}}=\mathbf{P}^{\mathrm{T}}$, and $\mathbf{Z}=\mathbf{P}$ are substituted into equation (34) and we obtain

$$\mathbf{P}^{\mathrm{T}}\mathbf{P}^{-1}\mathbf{P}-\mathbf{P}^{\mathrm{T}}\mathbf{P}^{-\mathrm{T}}\dot{\mathbf{A}}(\mathbf{X})\mathbf{P}^{-1}\mathbf{P}+\mathbf{P}^{\mathrm{T}}\mathbf{P}^{-\mathrm{T}}\mathbf{P}\geq\mathbf{P}^{\mathrm{T}}\Pi\mathbf{P}. \tag{36}$$

Since $\mathbf{P}^{\mathrm{T}}\mathbf{P}^{-\mathrm{T}}=\mathbf{I}_{6\times6}$ and $\mathbf{P}^{-1}\mathbf{P}=\mathbf{I}_{6\times6}$, equation (35) can be simplified as

$$\mathbf{P}^{\mathrm{T}}-\dot{\mathbf{A}}(\mathbf{X})+\mathbf{P}\geq\mathbf{P}^{\mathrm{T}}\Pi\mathbf{P}. \tag{37}$$

That is, $\mathbf{Z}^{\mathrm{T}}-\dot{\mathbf{A}}(\mathbf{X})+\mathbf{Z}\geq\mathbf{Z}^{\mathrm{T}}\Pi\mathbf{Z}$, $\mathbf{Z}^{\mathrm{T}}+\mathbf{Z}-\mathbf{Z}^{\mathrm{T}}\Pi\mathbf{Z}\geq\dot{\mathbf{A}}(\mathbf{X})$.

Set $\|\dot{\mathbf{A}}(\mathbf{X})\|\leq\eta$, then $\dot{\mathbf{A}}(\mathbf{X})\leq\eta\mathbf{I}_{6\times6}$. If the above equation is tenable, sufficient conditions for establishment of equation (37) are

$$\mathbf{Z}^{\mathrm{T}}+\mathbf{Z}-\mathbf{Z}^{\mathrm{T}}\Pi\mathbf{Z}\geq\eta\mathbf{I}_{6\times6}. \tag{38}$$

That is, $\mathbf{Z}^{\mathrm{T}}+\mathbf{Z}-\mathbf{Z}^{\mathrm{T}}\Pi\mathbf{Z}-\eta\mathbf{I}_{6\times6}\geq0$.

Theorem 1. *The Schur complement property of matrices can transform nonlinear matrix inequalities into LMI problems. Schur complement theorem: assuming that* $\mathbf{C}_1$ *is a positive definite matrix, then* $\mathbf{A}_1-\mathbf{B}_1\mathbf{C}_1^{-1}\mathbf{B}_1^{T}\geq0$ *is equivalent to* $\begin{bmatrix}\mathbf{A}_1 & \mathbf{B}_1\\ \mathbf{B}_1^{T} & \mathbf{C}_1\end{bmatrix}\geq0$.

Hence, equation (37) is equivalent to $\begin{bmatrix}\mathbf{Z}^{\mathrm{T}}+\mathbf{Z}-\eta\mathbf{I}_{6\times6} & \mathbf{Z}^{\mathrm{T}}\\ \mathbf{Z} & \Pi^{-1}\end{bmatrix}\geq0$.

By using the YALMIP toolbox in MATLAB to get $\mathbf{P}$, the validity of the solution to the inequality depends on η and Π. The smaller the values of η and Π are, the easier it is to get the effective solution.

4. Backstepping Sliding Mode Robust Control Design

The backstepping design method is a systematical controller synthesis method for uncertain systems. It is a regression design method combining the selection of Lyapunov functions with the design of the controller. The backstepping method has been applied extensively because of the unique superiority in dealing with the nonlinear control problem [18–23]. It begins with the lowest order differential equations of the system, introduces the concept of virtual control, and designs the virtual control to meet the requirements step by step. Finally, the real control law is designed. The advantage of sliding mode control is that it can get over the uncertainties of the system, which has strong robustness to the disturbance and unmodeled dynamics, and has good effect especially on the control of the nonlinear system.

Therefore, based on the above mentioned designed nonlinear disturbance observer to observe the total disturbance $\mathbf{D}(\mathbf{X},\dot{X},\ddot{X})$, the backstepping control method is adapted and the sliding mode term is introduced to overcome disturbance and enhance the robustness of the controller.

Firstly, let $\mathbf{X}_1=\mathbf{X}$ and $\mathbf{X}_2=\dot{X}$, and the dynamic equation (16) can be simplified as follows:

$$\begin{cases}\dot{X}_1=\mathbf{X}_2,\\ \dot{X}_2=\mathbf{A}^{-1}(\mathbf{X})\left(-\mathbf{B}(\mathbf{X})\mathbf{X}_2+\mathbf{J}^{\mathrm{T}}\boldsymbol{\tau}+\mathbf{D}(\mathbf{X},\dot{X},\ddot{X})-\mu\mathbf{w}_g\right).\end{cases} \tag{39}$$

Set the ideal pose to be $\mathbf{X}_d$ and take the tracking error as $\mathbf{e}=\mathbf{X}-\mathbf{X}_d$; then, $\dot{e}=\mathbf{X}-\dot{X}_d$; that is, $\dot{e}=\mathbf{X}_2-\dot{X}_d$. The following sliding mode function is defined:

$$\mathbf{s}=\dot{e}+\Gamma\mathbf{e}, \tag{40}$$

where $\Gamma=\mathrm{diag}[\,\lambda_1\ \ \lambda_2\ \ \cdots\ \ \lambda_6\,]$, $\lambda_i>0$, $i=1,2,\ldots,6$.

Let $\mathbf{z}_1=\mathbf{e}$ and define $\mathbf{z}_2=\mathbf{s}=\dot{e}+\Gamma\mathbf{e}=\dot{z}_1+\Gamma\mathbf{z}_1$, where $\mathbf{z}_2$ is the virtual control item, $\dot{z}_1=\mathbf{z}_2-\Gamma\mathbf{z}_1$.

Proof. A Lyapunov function is defined as

$$\mathbf{V}_1=\frac{1}{2}\mathbf{e}^{\mathrm{T}}\mathbf{e}=\frac{1}{2}\mathbf{z}_1^{\mathrm{T}}\mathbf{z}_1. \tag{41}$$

□

Then,

$$\dot{\mathbf{V}}_1 = \mathbf{z}_1^{\mathrm{T}}\dot{z}_1 = \mathbf{z}_1^{\mathrm{T}}(\mathbf{z}_2 - \Gamma\mathbf{z}_1) = \mathbf{z}_1^{\mathrm{T}}\mathbf{z}_2 - \mathbf{z}_1^{\mathrm{T}}\Gamma\mathbf{z}_1. \tag{42}$$

Define the switching function as

$$\mathbf{s}_1 = \kappa\mathbf{z}_1 + \mathbf{z}_2 = \kappa\mathbf{e} + \dot{e} + \Gamma\mathbf{e} = \dot{e} + (\kappa + \Gamma)\mathbf{e} = \dot{z}_1 + (\kappa + \Gamma)\mathbf{z}_1, \tag{43}$$

where $\kappa = \mathrm{diag}[\ \xi_1\ \ \xi_2\ \ \cdots\ \ \xi_6\ ]$, $\xi_i > 0$, $i = 1, 2, \ldots, 6$.

Let $\vartheta = (\kappa + \Gamma)$, since $\vartheta = \kappa + \Gamma = \mathrm{diag}[\ \lambda_1 + \xi_1\ \ \lambda_2 + \xi_2\ \cdots\ \lambda_6 + \xi_6\ ]$, $\lambda_i + \xi_i > 0$, $i = 1, 2, \ldots, 6$; if $\mathbf{s}_1 = 0$, then $\mathbf{z}_1 = 0$, $\mathbf{z}_2 = 0$, and $\dot{V}_1 \le 0$.

Proof. For the sake of making the control law free of acceleration term $\ddot{X}$, $\dot{X}_r = \dot{X} - \mathbf{s}_1$ is defined; then, the derivative of $\mathbf{X}_r$ is

$$\begin{aligned}\dot{X}_r &= \dot{X} - \mathbf{s}_1 = \dot{X} - (\dot{e} + (\kappa + \Gamma)\mathbf{e}) \\ &= \dot{X} - \dot{e} - (\kappa + \Gamma)\mathbf{e} = \dot{X}_d - (\kappa + \Gamma)\mathbf{e}, \\ \ddot{X}_r &= \ddot{X}_d - (\kappa + \Gamma)\dot{e}.\end{aligned} \tag{44}$$

□

Therefore, it is guaranteed that $\ddot{X}_r$ does not contain the acceleration item $\ddot{X}$.

As a result, $\dot{s}_1 = \ddot{X} - \ddot{X}_d + \vartheta\dot{e}$, then

$$\begin{aligned}\dot{s}_1 &= \ddot{X} - \ddot{X}_r = \ddot{X} - \ddot{X}_d + (\kappa + \Gamma)\dot{e} = \ddot{X} - \ddot{X}_d + \vartheta\dot{e} \\ &= \mathbf{A}^{-1}(\mathbf{X})\left(-\mathbf{B}(\mathbf{X})\mathbf{X}_2 + \mathbf{J}^{\mathrm{T}}\boldsymbol{\tau} + \mathbf{D}(\mathbf{X}, \dot{X}, \ddot{X}) - \mu\mathbf{w}_g\right) - \ddot{X}_r, \\ \mathbf{A}(\mathbf{X})\dot{s}_1 &= \mathbf{A}(\mathbf{X})\left(\mathbf{A}^{-1}(\mathbf{X})\left(-\mathbf{B}(\mathbf{X})\mathbf{X}_2 + \mathbf{J}^{\mathrm{T}}\boldsymbol{\tau} + \mathbf{D}(\mathbf{X}, \dot{X}, \ddot{X}) - \mu\mathbf{w}_g\right) - \ddot{X}_r\right) \\ &= -\mathbf{B}(\mathbf{X})\mathbf{X}_2 + \mathbf{J}^{\mathrm{T}}\boldsymbol{\tau} + \mathbf{D}(\mathbf{X}, \dot{X}, \ddot{X}) - \mu\mathbf{w}_g - \mathbf{A}(\mathbf{X})\ddot{X}_r.\end{aligned} \tag{45}$$

Define the following Lyapunov function as follows:

$$\mathbf{V}_2 = \mathbf{V}_1 + \frac{1}{2}\mathbf{s}_1^{\mathrm{T}}\mathbf{A}(\mathbf{X})\mathbf{s}_1 = \frac{1}{2}\mathbf{e}^{\mathrm{T}}\mathbf{e} + \frac{1}{2}\mathbf{s}_1^{\mathrm{T}}\mathbf{A}(\mathbf{X})\mathbf{s}_1 = \frac{1}{2}\mathbf{z}_1^{\mathrm{T}}\mathbf{z}_1 + \frac{1}{2}\mathbf{s}_1^{\mathrm{T}}\mathbf{A}(\mathbf{X})\mathbf{s}_1. \tag{46}$$

The derivative of $\mathbf{V}_2$ is

$$\begin{aligned}\dot{\mathbf{V}}_2 &= \dot{V}_1 + \mathbf{s}_1^{\mathrm{T}}\mathbf{A}(\mathbf{X})\dot{s}_1 + \frac{1}{2}\mathbf{s}_1^{\mathrm{T}}\dot{\mathbf{A}}(\mathbf{X})\mathbf{s}_1 \\ &= \mathbf{z}_1^{\mathrm{T}}\mathbf{z}_2 - \mathbf{z}_1^{\mathrm{T}}\Gamma\mathbf{z}_1 + \mathbf{s}_1^{\mathrm{T}}\mathbf{A}(\mathbf{X})(\kappa\dot{z}_1 + \dot{z}_2) + \frac{1}{2}\mathbf{s}_1^{\mathrm{T}}\dot{\mathbf{A}}(\mathbf{X})\mathbf{s}_1 \\ &= \mathbf{z}_1^{\mathrm{T}}\mathbf{z}_2 - \mathbf{z}_1^{\mathrm{T}}\Gamma\mathbf{z}_1 + \mathbf{s}_1^{\mathrm{T}}\left(-\mathbf{B}(\mathbf{X})\mathbf{X}_2 + \mathbf{J}^{\mathrm{T}}\boldsymbol{\tau} + \mathbf{D}(\mathbf{X}, \dot{X}, \ddot{X}) - \mu\mathbf{w}_g\right. \\ &\quad \left. - \mathbf{A}(\mathbf{X})\ddot{X}_r\right) + \frac{1}{2}\mathbf{s}_1^{\mathrm{T}}\dot{\mathbf{A}}(\mathbf{X})\mathbf{s}_1.\end{aligned} \tag{47}$$

Table 1: Positions of P_i and B_i.

Symbol	Coordinate (mm)
P_1	$(-208, 78, -1)^{\mathrm{T}}$
P_2	$(-208, -78, -1)^{\mathrm{T}}$
P_3	$(0, -27.7, -10.1)^{\mathrm{T}}$
P_4	$(0, 27.7, -10.1)^{\mathrm{T}}$
P_5	$(0, 27.7, 10.1)^{\mathrm{T}}$
P_6	$(-208, 78, 1)^{\mathrm{T}}$
P_7	$(-208, -78, 1)^{\mathrm{T}}$
P_8	$(0, -27.7, 10.1)^{\mathrm{T}}$
B_1	$(200, 415, -1280)^{\mathrm{T}}$
B_2	$(200, -415, -1280)^{\mathrm{T}}$
B_3	$(-300, -308, -1250)^{\mathrm{T}}$
B_4	$(-300, 308, -1250)^{\mathrm{T}}$
B_5	$(-315, 315, -70)^{\mathrm{T}}$
B_6	$(160, 415, -70)^{\mathrm{T}}$
B_7	$(160, -415, -70)^{\mathrm{T}}$
B_8	$(-315, -315, -70)^{\mathrm{T}}$

The parameter values in Table 2 are used for simulation analysis.

Table 2: Simulation parameter table.

Parameter	Value
$\mathbf{M}_0$	$7 * 10^{-5}\mathbf{I}_{8\times8}$
$\mathbf{C}_0$	$0.005\mathbf{I}_{8\times8}$
m	1.028 kg
μ	0.0025 pi
Γ	$15\mathbf{I}_{6\times6}$
g	$9.82\ \mathrm{m/s^2}$
κ	$5\mathbf{I}_{6\times6}$
η	2
χ	$5\mathbf{I}_{6\times6}$
P	$7.3361\mathbf{I}_{6\times6}$
Π	$0.01 * \mathrm{diag}[5\ 7\ 9\ 8\ 10\ 15]$
$\mathbf{K}_P$	$10^3 * \mathrm{diag}[3\ 11\ 12\ 0.15\ 0.12\ 0.25]$

According to equations (47) and (39), a backstepping sliding mode robust control law $\boldsymbol{\tau}$ is designed as follows:

$$\begin{aligned}\boldsymbol{\tau} &= \left(\mathbf{J}^{\mathrm{T}}\right)^{+}\left(\mathbf{A}(\mathbf{X})\left(\ddot{X}_d - \vartheta(\mathbf{z}_2 - \Gamma\mathbf{z}_1)\right) + \mathbf{B}(\mathbf{X})\left(\dot{X}_d - \vartheta\mathbf{z}_1\right) + \mu\mathbf{w}_g\right. \\ &\quad \left. - \chi\,\mathrm{sgn}\,\mathbf{s}_1 - \widehat{D}(\mathbf{X}, \dot{X}, \ddot{X})\right) \\ &= \left(\mathbf{J}^{\mathrm{T}}\right)^{+}\left(\mathbf{A}(\mathbf{X})\left(\ddot{X}_d - \vartheta\dot{e}\right) + \mathbf{B}(\mathbf{X})\left(\dot{X}_d - \vartheta\mathbf{e}\right) + \mu\mathbf{w}_g - \chi\mathrm{sgn}\,\mathbf{s}_1\right. \\ &\quad \left. - \widehat{D}(\mathbf{X}, \dot{X}, \ddot{X})\right) \\ &= \left(\mathbf{J}^{\mathrm{T}}\right)^{+}\left(\mathbf{A}(\mathbf{X})\ddot{X}_r + \mathbf{B}(\mathbf{X})\dot{X}_r + \mu\mathbf{w}_g - \chi\mathrm{sgn}\,\mathbf{s}_1 - \widehat{D}(\mathbf{X}, \dot{X}, \ddot{X})\right),\end{aligned} \tag{48}$$

where $\chi = \mathrm{diag}[\ \varepsilon_1\ \ \varepsilon_2\ \ \cdots\ \ \varepsilon_6\ ]$, $\varepsilon_i > 0$, $i = 1, 2, \ldots, 6$.

The design control law is substituted into equation (47), and we obtain

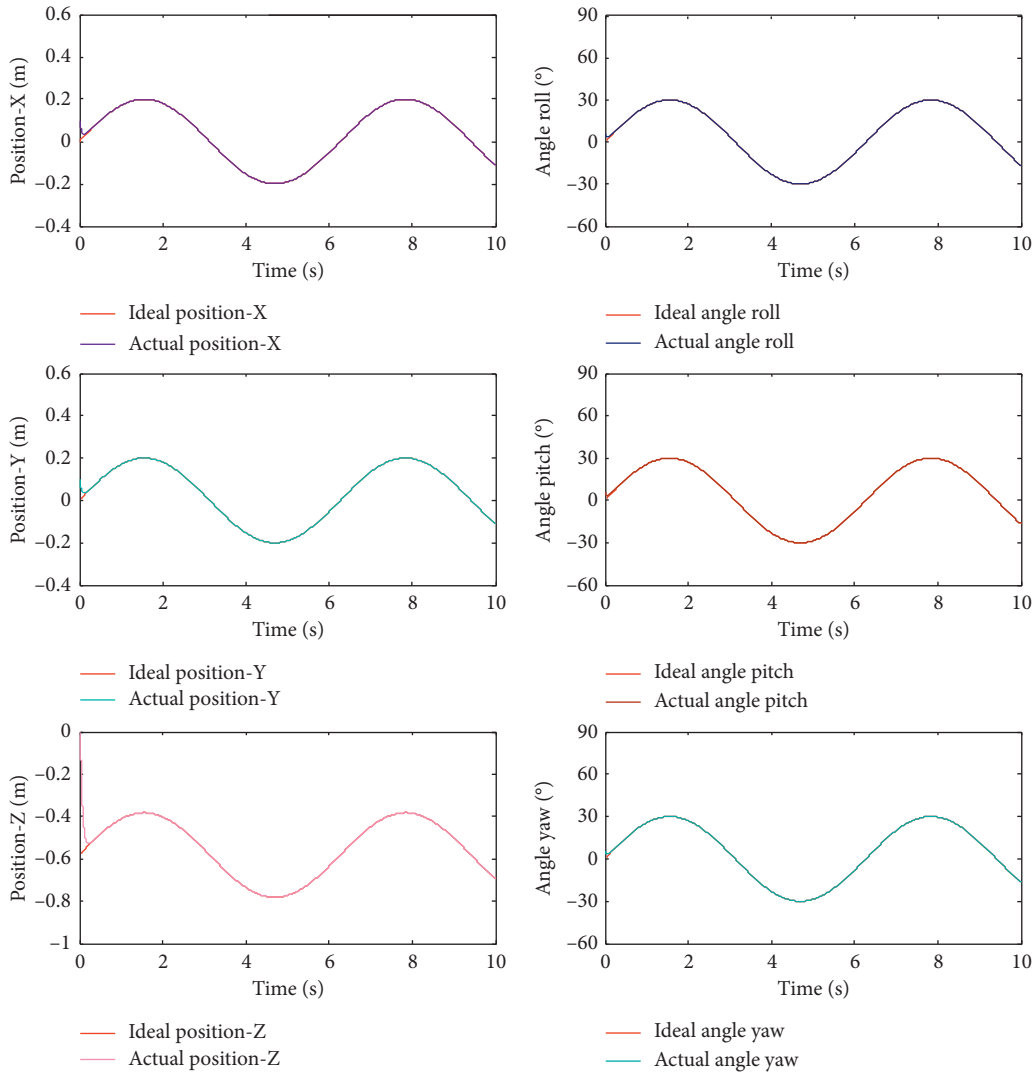

Figure 3: Pose curve.

$$
\begin{aligned}
\dot{V}_2 = {} & \dot{V}_1 + \mathbf{s}_1^{\mathrm{T}}\mathbf{A}(\mathbf{X})\dot{s}_1 + \frac{1}{2}\mathbf{s}_1^{\mathrm{T}}\dot{\mathbf{A}}(\mathbf{X})\mathbf{s}_1 \\
= {} & \mathbf{z}_1^{\mathrm{T}}\mathbf{z}_2 - \mathbf{z}_1^{\mathrm{T}}\Gamma\mathbf{z}_1 + \mathbf{s}_1^{\mathrm{T}}\mathbf{A}(\mathbf{X})\Big(\mathbf{A}^{-1}(\mathbf{X})\Big(-\mathbf{B}(\mathbf{X})\mathbf{X}_2 + \mathbf{J}^{\mathrm{T}}\Big(\mathbf{J}^{\mathrm{T}}\Big)^{+}\Big(\mathbf{A}(\mathbf{X})\ddot{X}_r + \mathbf{B}(\mathbf{X})\dot{X}_r + \mu\mathbf{w}_g - \chi\operatorname{sgn}\mathbf{s}_1 - \widehat{D}(\mathbf{X},\dot{X},\ddot{X})\Big) + \mathbf{D}(\mathbf{X},\dot{X},\ddot{X}) - \mu\mathbf{w}_g\Big) \\
& - \ddot{X}_r\Big) + \frac{1}{2}\mathbf{s}_1^{\mathrm{T}}\dot{\mathbf{A}}(\mathbf{X})\mathbf{s}_1 \\
= {} & \mathbf{z}_1^{\mathrm{T}}\mathbf{z}_2 - \mathbf{z}_1^{\mathrm{T}}\Gamma\mathbf{z}_1 + \mathbf{s}_1^{\mathrm{T}}\mathbf{A}(\mathbf{X})\Big(\mathbf{A}^{-1}(\mathbf{X})\Big(-\mathbf{B}(\mathbf{X})\mathbf{X}_2 + \Big(\mathbf{A}(\mathbf{X})\ddot{X}_r + \mathbf{B}(\mathbf{X})\dot{X}_r + \mu\mathbf{w}_g - \chi\operatorname{sgn}\mathbf{s}_1 - \widehat{D}(\mathbf{X},\dot{X},\ddot{X})\Big) + \mathbf{D}(\mathbf{X},\dot{X},\ddot{X}) - \mu\mathbf{w}_g\Big) - \ddot{X}_r\Big) \\
& + \frac{1}{2}\mathbf{s}_1^{\mathrm{T}}\dot{\mathbf{A}}(\mathbf{X})\mathbf{s}_1 \\
= {} & \mathbf{z}_1^{\mathrm{T}}\mathbf{z}_2 - \mathbf{z}_1^{\mathrm{T}}\Gamma\mathbf{z}_1 + \mathbf{s}_1^{\mathrm{T}}\mathbf{A}(\mathbf{X})\Big(\mathbf{A}^{-1}(\mathbf{X})\Big(-\mathbf{B}(\mathbf{X})\dot{X} + \mathbf{B}(\mathbf{X})\dot{X}_r - \chi\operatorname{sgn}\mathbf{s}_1 + \widetilde{D}(\mathbf{X},\dot{X},\ddot{X})\Big)\Big) + \frac{1}{2}\mathbf{s}_1^{\mathrm{T}}\dot{\mathbf{A}}(\mathbf{X})\mathbf{s}_1 \\
= {} & \mathbf{z}_1^{\mathrm{T}}\mathbf{z}_2 - \mathbf{z}_1^{\mathrm{T}}\Gamma\mathbf{z}_1 + \mathbf{s}_1^{\mathrm{T}}\mathbf{A}(\mathbf{X})\Big(\mathbf{A}^{-1}(\mathbf{X})\Big(-\mathbf{B}(\mathbf{X})\mathbf{s}_1 - \chi\operatorname{sgn}\mathbf{s}_1 + \widetilde{D}(\mathbf{X},\dot{X},\ddot{X})\Big)\Big) + \frac{1}{2}\mathbf{s}_1^{\mathrm{T}}\dot{\mathbf{A}}(\mathbf{X})\mathbf{s}_1 \\
= {} & \mathbf{z}_1^{\mathrm{T}}\mathbf{z}_2 - \mathbf{z}_1^{\mathrm{T}}\Gamma\mathbf{z}_1 - \mathbf{s}_1^{\mathrm{T}}\mathbf{A}(\mathbf{X})\mathbf{A}^{-1}(\mathbf{X})\mathbf{B}(\mathbf{X})\mathbf{s}_1 - \mathbf{s}_1^{\mathrm{T}}\mathbf{A}(\mathbf{X})\mathbf{A}^{-1}(\mathbf{X})\chi\operatorname{sgn}\mathbf{s}_1 + \mathbf{s}_1^{\mathrm{T}}\Big(\mathbf{A}(\mathbf{X})\mathbf{A}^{-1}(\mathbf{X})\widetilde{D}(\mathbf{X},\dot{X},\ddot{X})\Big) + \frac{1}{2}\mathbf{s}_1^{\mathrm{T}}\dot{\mathbf{A}}(\mathbf{X})\mathbf{s}_1 \\
= {} & \mathbf{z}_1^{\mathrm{T}}\mathbf{z}_2 - \mathbf{z}_1^{\mathrm{T}}\Gamma\mathbf{z}_1 - \mathbf{s}_1^{\mathrm{T}}\Big(\mathbf{B}(\mathbf{X})\mathbf{s}_1 - \mathbf{s}_1^{\mathrm{T}}\chi\operatorname{sgn}\mathbf{s}_1 + \mathbf{s}_1^{\mathrm{T}}\widetilde{D}(\mathbf{X},\dot{X},\ddot{X})\Big) + \frac{1}{2}\mathbf{s}_1^{\mathrm{T}}\dot{\mathbf{A}}(\mathbf{X})\mathbf{s}_1,
\end{aligned}
$$

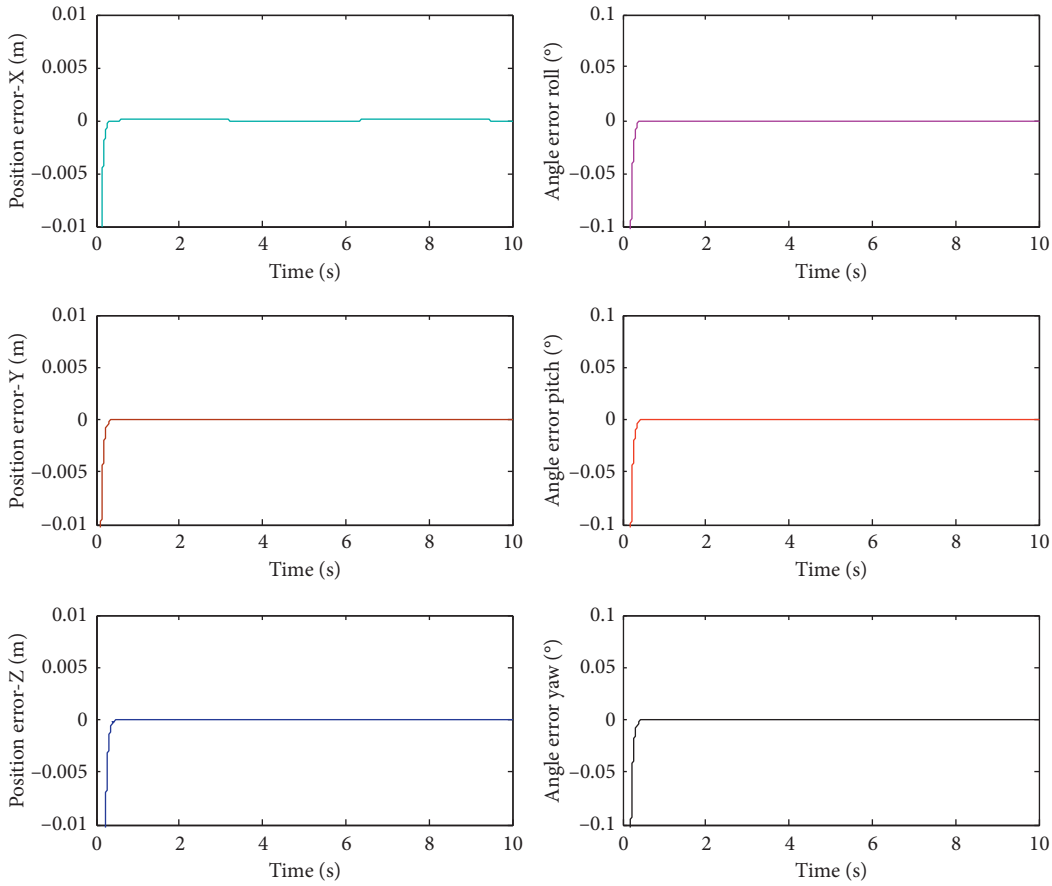

Figure 4: Pose error curve.

$$\begin{aligned}\dot{V}_2 &\le \mathbf{z}_1^{\mathrm{T}}\mathbf{z}_2 - \mathbf{z}_1^{\mathrm{T}}\Gamma\mathbf{z}_1 - \mathbf{s}_1^{\mathrm{T}}(\mathbf{X})\mathbf{s}_1 - \mathbf{s}_1^{\mathrm{T}}\chi\operatorname{sgn}\mathbf{s}_1 + \frac{1}{2}\mathbf{s}_1^{\mathrm{T}}\dot{\mathbf{A}}(\mathbf{X})\mathbf{s}_1 + \mathbf{s}_1^{\mathrm{T}}\mathbf{K}_P\mathbf{s}_1 \\ &= \mathbf{z}_1^{\mathrm{T}}\mathbf{z}_2 - \mathbf{z}_1^{\mathrm{T}}\Gamma\mathbf{z}_1 - \mathbf{s}_1^{\mathrm{T}}\left(\mathbf{B}(\mathbf{X}) - \frac{\dot{\mathbf{A}}(\mathbf{X})}{2} + \mathbf{K}_P\right)\mathbf{s}_1 - \mathbf{s}_1^{\mathrm{T}}\chi\operatorname{sgn}\mathbf{s}_1 \\ &= -\left(\mathbf{z}_1^{\mathrm{T}}\Gamma\mathbf{z}_1 - \mathbf{z}_1^{\mathrm{T}}\mathbf{z}_2 + \mathbf{s}_1^{\mathrm{T}}\left(\mathbf{B}(\mathbf{X}) - \frac{\dot{\mathbf{A}}(\mathbf{X})}{2} + \mathbf{K}_P\right)\mathbf{s}_1\right) - \mathbf{s}_1^{\mathrm{T}}\chi\operatorname{sgn}\mathbf{s}_1, \end{aligned} \tag{49}$$

where $\mathbf{A}(\mathbf{X})\mathbf{A}^{-1}(\mathbf{X}) = \mathbf{I}_{6\times 6}$, $\mathbf{K}_P = \operatorname{diag}[\,K_1 \;\; K_2 \;\; \cdots \;\; K_6\,]$, and $K_i > 0$, $i = 1, 2, \ldots, 6$.

Take $\mathbf{Y}$ as shown in equation (50) as follows:

$$\mathbf{Y} = \begin{bmatrix} \Gamma + \kappa^{\mathrm{T}}\left(\mathbf{B}(\mathbf{X}) - \dfrac{\dot{\mathbf{A}}(\mathbf{X})}{2} + \mathbf{K}_P\right)\kappa & \left(\mathbf{B}(\mathbf{X}) - \dfrac{\dot{\mathbf{A}}(\mathbf{X})}{2} + \mathbf{K}_P\right)\kappa - \dfrac{1}{2} \\ \left(\mathbf{B}(\mathbf{X}) - \dfrac{\dot{\mathbf{A}}(\mathbf{X})}{2} + \mathbf{K}_P\right)\kappa - \dfrac{1}{2} & \left(\mathbf{B}(\mathbf{X}) - \dfrac{\dot{\mathbf{A}}(\mathbf{X})}{2} + \mathbf{K}_P\right) \end{bmatrix}. \tag{50}$$

Let $\mathbf{x}^{\mathrm{T}} = \left[\,\mathbf{z}_1^{\mathrm{T}} \;\; \mathbf{z}_2^{\mathrm{T}}\,\right]$, then

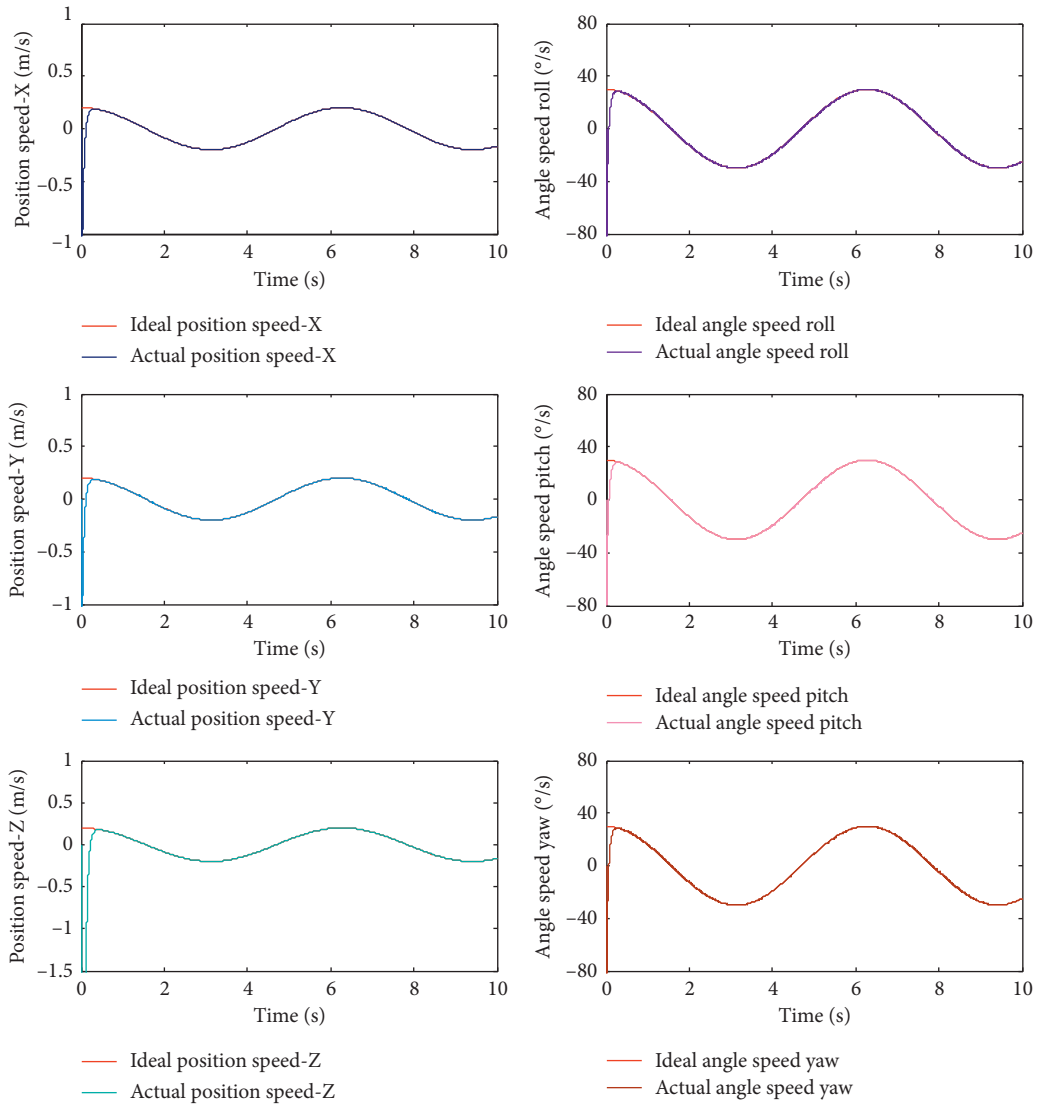

Figure 5: Pose speed curve.

$$\mathbf{x}^{\mathrm{T}}\mathbf{Y}\mathbf{x} = \mathbf{x}^{\mathrm{T}}\begin{bmatrix} \Gamma + \kappa^{\mathrm{T}}\left(\mathbf{B}(\mathbf{X}) - \dfrac{\dot{\mathbf{A}}(\mathbf{X})}{2} + \mathbf{K}_P\right)\kappa & \left(\mathbf{B}(\mathbf{X}) - \dfrac{\dot{\mathbf{A}}(\mathbf{X})}{2} + \mathbf{K}_P\right)\kappa - \dfrac{1}{2} \\ \left(\mathbf{B}(\mathbf{X}) - \dfrac{\dot{\mathbf{A}}(\mathbf{X})}{2} + \mathbf{K}_P\right)\kappa - \dfrac{1}{2} & \left(\mathbf{B}(\mathbf{X}) - \dfrac{\dot{\mathbf{A}}(\mathbf{X})}{2} + \mathbf{K}_P\right) \end{bmatrix}\mathbf{x}$$

$$= \begin{bmatrix} \mathbf{z}_1^{\mathrm{T}} & \mathbf{z}_2^{\mathrm{T}} \end{bmatrix}\begin{bmatrix} \Gamma + \kappa^{\mathrm{T}}\left(\mathbf{B}(\mathbf{X}) - \dfrac{\dot{\mathbf{A}}(\mathbf{X})}{2} + \mathbf{K}_P\right)\kappa & \left(\mathbf{B}(\mathbf{X}) - \dfrac{\dot{\mathbf{A}}(\mathbf{X})}{2} + \mathbf{K}_P\right)\kappa - \dfrac{1}{2} \\ \left(\mathbf{B}(\mathbf{X}) - \dfrac{\dot{\mathbf{A}}(\mathbf{X})}{2} + \mathbf{K}_P\right)\kappa - \dfrac{1}{2} & \left(\mathbf{B}(\mathbf{X}) - \dfrac{\dot{\mathbf{A}}(\mathbf{X})}{2} + \mathbf{K}_P\right) \end{bmatrix}\begin{bmatrix} \mathbf{z}_1 \\ \mathbf{z}_2 \end{bmatrix}$$

$$= \left[\mathbf{z}_1^{\mathrm{T}}\left(\Gamma + \kappa^{\mathrm{T}}\left(\mathbf{B}(\mathbf{X}) - \frac{\dot{\mathbf{A}}(\mathbf{X})}{2} + \mathbf{K}_P\right)\kappa\right) + \mathbf{z}_2^{\mathrm{T}}\left(\left(\mathbf{B}(\mathbf{X}) - \frac{\dot{\mathbf{A}}(\mathbf{X})}{2} + \mathbf{K}_P\right)\kappa - \frac{1}{2}\right)\mathbf{z}_1^{\mathrm{T}}\left(\left(\mathbf{B}(\mathbf{X}) - \frac{\dot{\mathbf{A}}(\mathbf{X})}{2} + \mathbf{K}_P\right)\kappa - \frac{1}{2}\right)\right.$$
$$\left. + \mathbf{z}_2^{\mathrm{T}}\left(\mathbf{B}(\mathbf{X}) - \frac{\dot{\mathbf{A}}(\mathbf{X})}{2} + \mathbf{K}_P\right)\right]\begin{bmatrix} \mathbf{z}_1 \\ \mathbf{z}_2 \end{bmatrix},$$

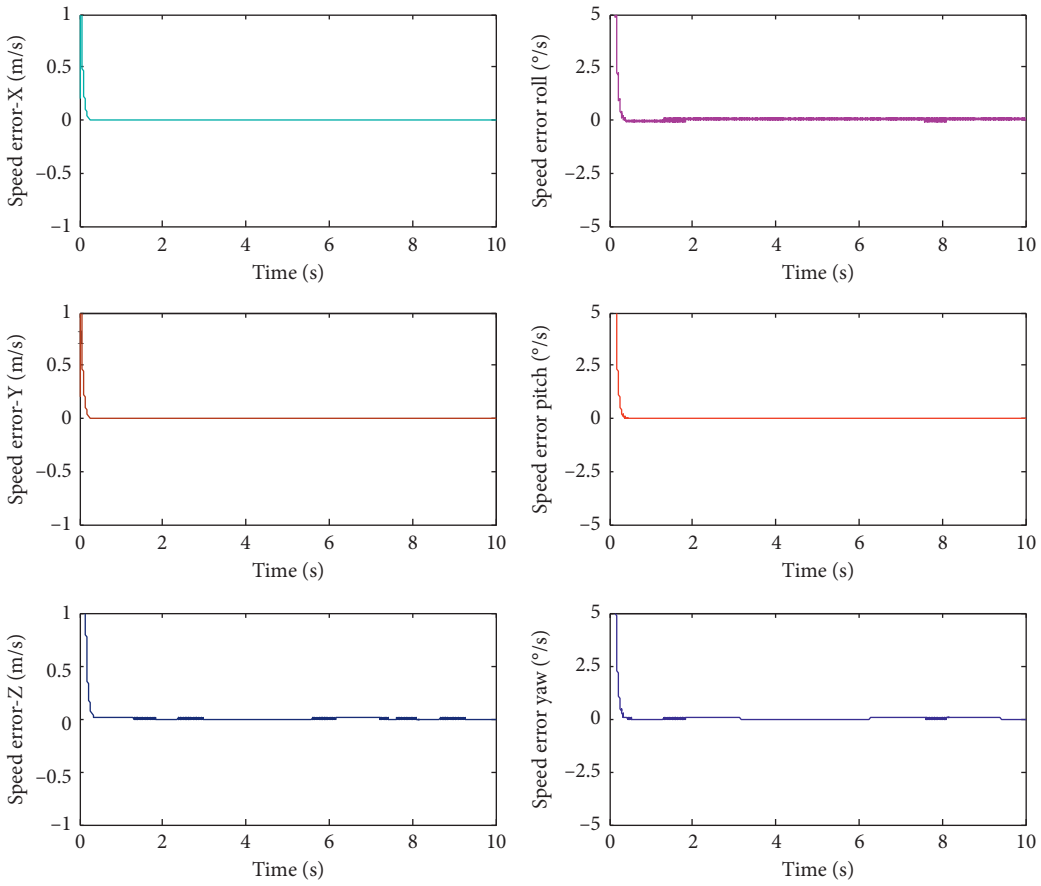

Figure 6: Pose speed error curve.

$$= \mathbf{z}_1^{\mathrm{T}}\left(\Gamma + \kappa^{\mathrm{T}}\left(\mathbf{B}(\mathbf{X}) - \frac{\dot{\mathbf{A}}(\mathbf{X})}{2} + \mathbf{K}_P\right)\kappa\right)\mathbf{z}_1 + \mathbf{z}_2^{\mathrm{T}}\left(\left(\mathbf{B}(\mathbf{X}) - \frac{\dot{\mathbf{A}}(\mathbf{X})}{2} + \mathbf{K}_P\right)\kappa - \frac{1}{2}\right)\mathbf{z}_1 + \mathbf{z}_1^{\mathrm{T}}\left(\left(\mathbf{B}(\mathbf{X}) - \frac{\dot{\mathbf{A}}(\mathbf{X})}{2} + \mathbf{K}_P\right)\kappa - \frac{1}{2}\right)\mathbf{z}_2$$

$$+ \mathbf{z}_2^{\mathrm{T}}\left(\mathbf{B}(\mathbf{X}) - \frac{\dot{\mathbf{A}}(\mathbf{X})}{2} + \mathbf{K}_P\right)\mathbf{z}_2 = \mathbf{z}_1^{\mathrm{T}}\left(\Gamma + \kappa^{\mathrm{T}}\left(\mathbf{B}(\mathbf{X}) - \frac{\dot{\mathbf{A}}(\mathbf{X})}{2} + \mathbf{K}_P\right)\kappa\right)\mathbf{z}_1 + 2\mathbf{z}_1^{\mathrm{T}}\left(\left(\mathbf{B}(\mathbf{X}) - \frac{\dot{\mathbf{A}}(\mathbf{X})}{2} + \mathbf{K}_P\right)\kappa - \frac{1}{2}\right)\mathbf{z}_2$$

$$+ \mathbf{z}_2^{\mathrm{T}}\left(\mathbf{B}(\mathbf{X}) - \frac{\dot{\mathbf{A}}(\mathbf{X})}{2} + \mathbf{K}_P\right)\mathbf{z}_2 = \mathbf{z}_1^{\mathrm{T}}\Gamma\mathbf{z}_1 - \mathbf{z}_1^{\mathrm{T}}\mathbf{z}_2 + \mathbf{z}_1^{\mathrm{T}}\kappa^{\mathrm{T}}\left(\mathbf{B}(\mathbf{X}) - \frac{\dot{\mathbf{A}}(\mathbf{X})}{2} + \mathbf{K}_P\right)\kappa\mathbf{z}_1 + 2\mathbf{z}_1^{\mathrm{T}}\left(\mathbf{B}(\mathbf{X}) - \frac{\dot{\mathbf{A}}(\mathbf{X})}{2} + \mathbf{K}_P\right)\kappa\mathbf{z}_2$$

$$+ \mathbf{z}_2^{\mathrm{T}}\left(\mathbf{B}(\mathbf{X}) - \frac{\dot{\mathbf{A}}(\mathbf{X})}{2} + \mathbf{K}_P\right)\mathbf{z}_2 = \mathbf{z}_1^{\mathrm{T}}\Gamma\mathbf{z}_1 - \mathbf{z}_1^{\mathrm{T}}\mathbf{z}_2 + (\kappa\mathbf{z}_1 + \mathbf{z}_2)^{\mathrm{T}}\left(\mathbf{B}(\mathbf{X}) - \frac{\dot{\mathbf{A}}(\mathbf{X})}{2} + \mathbf{K}_P\right)(\kappa\mathbf{z}_1 + \mathbf{z}_2) = \mathbf{z}_1^{\mathrm{T}}\Gamma\mathbf{z}_1 - \mathbf{z}_1^{\mathrm{T}}\mathbf{z}_2$$

$$+ \mathbf{s}_1^{\mathrm{T}}\left(\mathbf{B}(\mathbf{X}) - \frac{\dot{\mathbf{A}}(\mathbf{X})}{2} + \mathbf{K}_P\right)\mathbf{s}_1. \tag{51}$$

If $\mathbf{Y}$ is a positive definite matrix, $\mathbf{x}^{\mathrm{T}}\mathbf{Y}\mathbf{x} > 0$; then, $\dot{V}_2 \le -\mathbf{x}^{\mathrm{T}}\mathbf{Y}\mathbf{x} - \mathbf{s}_1{}^{\mathrm{T}}\chi\operatorname{sgn}\mathbf{s}_1 \le 0$.

According to the positive definite discriminant method of block matrix, suitable values $(\Gamma, \kappa, \mathbf{K}_P)$ are selected to ensure that $\mathbf{Y}$ is a positive definite matrix; therefore, $\dot{V}_2 \le 0$.

Proof. Design the Lyapunov function of the closed-loop system as

$$V = V_2 + V_0 = V_1 + \frac{1}{2}\mathbf{s}_1{}^{\mathrm{T}}\mathbf{A}(\mathbf{X})\mathbf{s}_1 + V_0. \tag{52}$$

The derivative of V can be derived as

$$\dot{V} = \dot{V}_2 + \dot{V}_0 = \dot{V}_1 + \mathbf{s}_1^{\mathrm{T}}\mathbf{A}(\mathbf{X})\dot{s}_1 + \frac{1}{2}\mathbf{s}_1^{\mathrm{T}}\dot{\mathbf{A}}(\mathbf{X})\mathbf{s}_1 + \dot{V}_0. \tag{53}$$

□

Because of $\dot{V}_2 \le 0$ and $\dot{V}_0 \le 0$, $\dot{V} \le 0$.Therefore, the backstepping sliding mode robust control system is asymptotically stable.

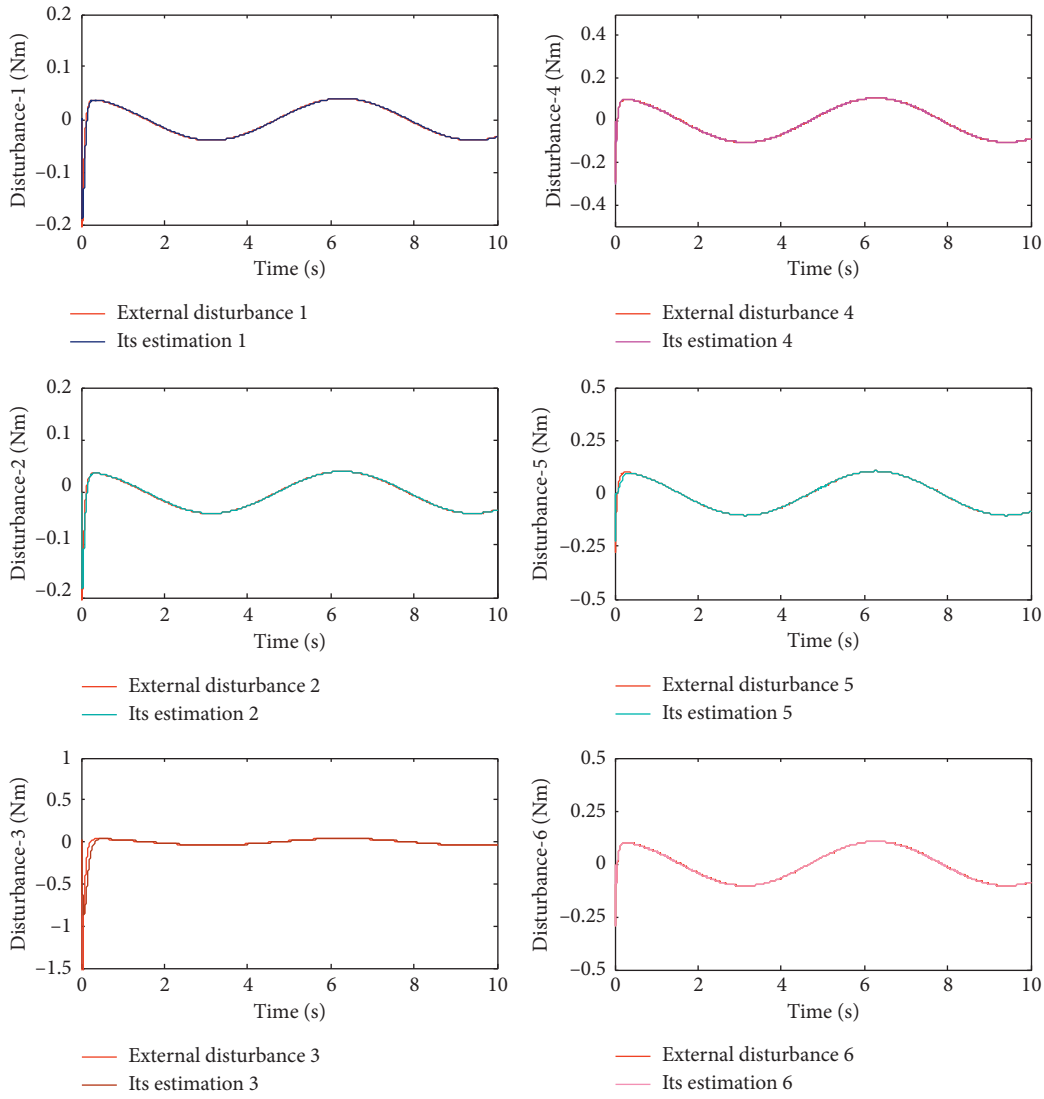

Figure 7: Disturbance observation results.

5. Simulation Experiments

For the sake of verifying the effectiveness of the proposed control approach, simulation experiments are implemented on the WDPR, as shown in Figure 1. The WDPR is used to do 6-DOF motion for the simulation experiments. The desired pose of the end-effector is set as follows:

$$X = [0.2 \times \sin(t); 0.2 \times \sin(t); 0.2 \times \sin(t) - 0.582; (\text{pi}/6) \times \sin(t); (\text{pi}/6) \times \sin(t); (\text{pi}/6) \times \sin(t)]. \quad (54)$$

Taking MATLAB/SIMULINK as the simulation software, according to the task nature and motion characteristics of WDPR, a simulation main program diagram of the backstepping sliding mode robust control is established.

The coordinate points of WDPR: the positions of P_i (the connecting point of the end-effector) and B_i (the hinge point of the pulley) ($i = 1 \sim 8$) are as shown in Table 1.

The mass of the end-effector (aircraft model) is 1.028 kg; $\mathbf{Y}$ is a positive definite matrix when Γ, κ, and $\mathbf{K}_P$ and take the values in Table 2. When $\eta = 2$, $\chi = 5\mathbf{I}_{6\times6}$, $\mathbf{P} = 7.3361\mathbf{I}_{6\times6}$, $\Pi = 0.01 * \text{diag}[5\ 7\ 9\ 8\ 10\ 15]$, and $\mathbf{K}_P = 10^3 * \text{diag}[3\ 11\ 12\ 0.15\ 0.12\ 0.25]$, the system is stable. In the simulation experiments, the ranges of pose error are set as follows: ±0.005 m and ±0.05°. The ranges of pose speed error are set as ±0.5 m/s and ±5°/s. The range of disturbance observation error is set as ±0.05. The simulation results are shown in Figures 3–11.

According to the simulation results of the pose, it can be concluded from Figure 3 that the curves of the theoretical pose and the actual pose coincide well with continuous 10 s; it can be seen from Figure 4 that the tracking error of the pose is basically 0, and the tracking effect is good.

It can be concluded from Figure 5 that the curve coincidence degree between the theoretical pose speed and the actual pose speed also tends to be consistent within continuous 10 s. As can be seen from Figure 6, the tracking error of pose speed tends to be 0 and the control precision is very high.

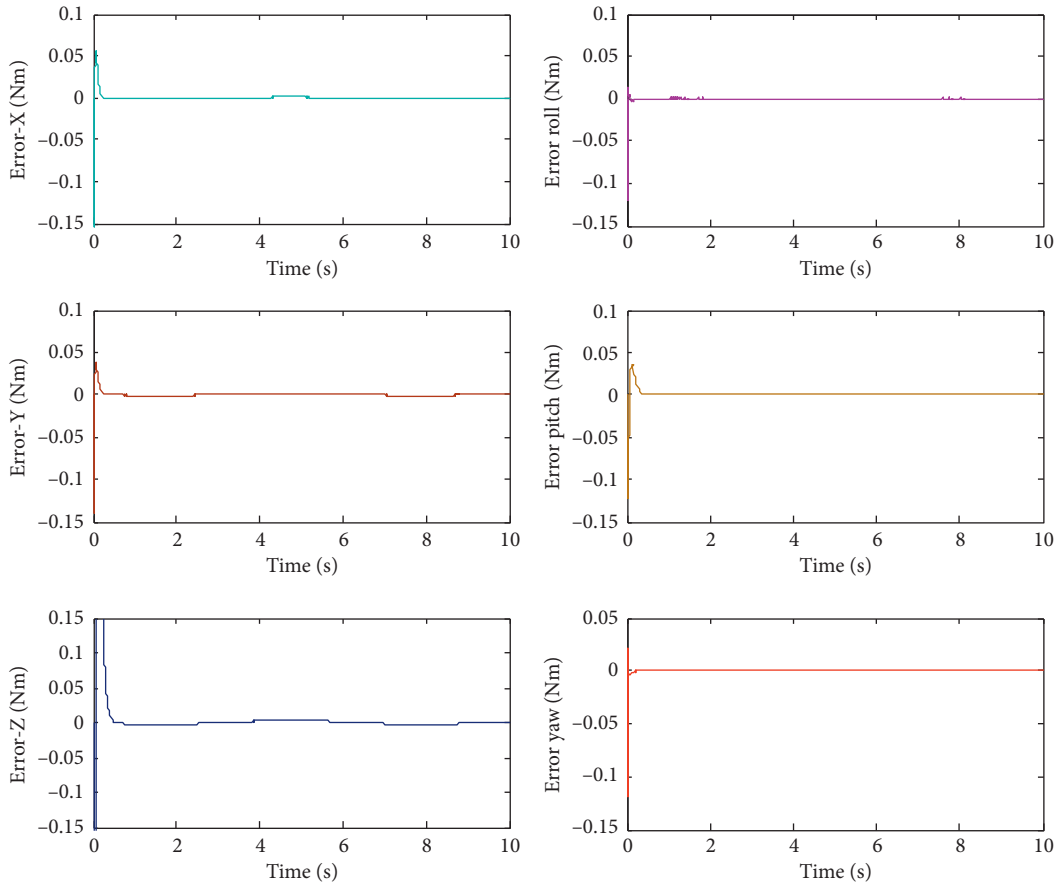

Figure 8: Disturbance observation error.

From the simulation results in Figure 7, it can be seen that the estimated disturbance observed by the nonlinear disturbance observer is extremely high in coincidence degree with the external disturbance; it can be concluded from Figure 8 that the observation error of the nonlinear disturbance observer is basically 0, which realizes the real-time estimation and real-time compensation of external disturbance.

It can be seen from Figure 9 that control inputs of the eight motors all vary within a certain range, which conforms to the physical significance of the design.

As can be seen from Figures 10 and 11, due to the six-degrees-of-freedom motion, there is no regularity in the variation of wire length and wire force, but the variation of eight-wire length and the variation of wire tension are within a certain range. The variation of wire length is smooth, and the variation of wire tension is gentle, which reduces the risk of broken wires.

The simulation results show that the equivalent disturbance can be observed through the proposed nonlinear disturbance observer, and the equivalent compensation is introduced into designed sliding mode control, which realizes the effective control of the disturbance. The tracking effect of the WDPR is good, and the control precision is high, which proves that the designed backstepping sliding mode robust control is practicable and dependable and satisfies motion tracking trajectory for the WDPR.

6. Prototype Experiments and Results

In order to further verify the correctness and effectiveness of the designed control law, the experimental verification is carried out on the WDPR prototype. The experimental mechanism is shown in Figure 1. The experimental mechanism mainly consists of control software and hardware system. The control software is programmed in C++ language on Visual Studio. The hardware system mainly includes an industrial personal computer (IPC), a motion controller, servo system, and mechanical structure. The motion controller is IMAC-HX, and it is powered by DC regulated power supply of DRP-240-24, as shown in Figure 12.

In order to validate the designed control method, first, the servo driver is set to the torque mode, and the connection of the hardware device and the configuration of the software environment are completed. In view of the established dynamic model and the robust control, the dynamic control software is designed to complete the control experiment of WDPR prototype. The control software mainly includes control main program, trajectory planning, inverse kinematics model, dynamic model, and other modules. Since the dynamic control software involves a large number of matrix operations for modeling and control, Eigen mathematical function library is used to deal with the operation of matrix vectors. The dynamic control software invokes the class

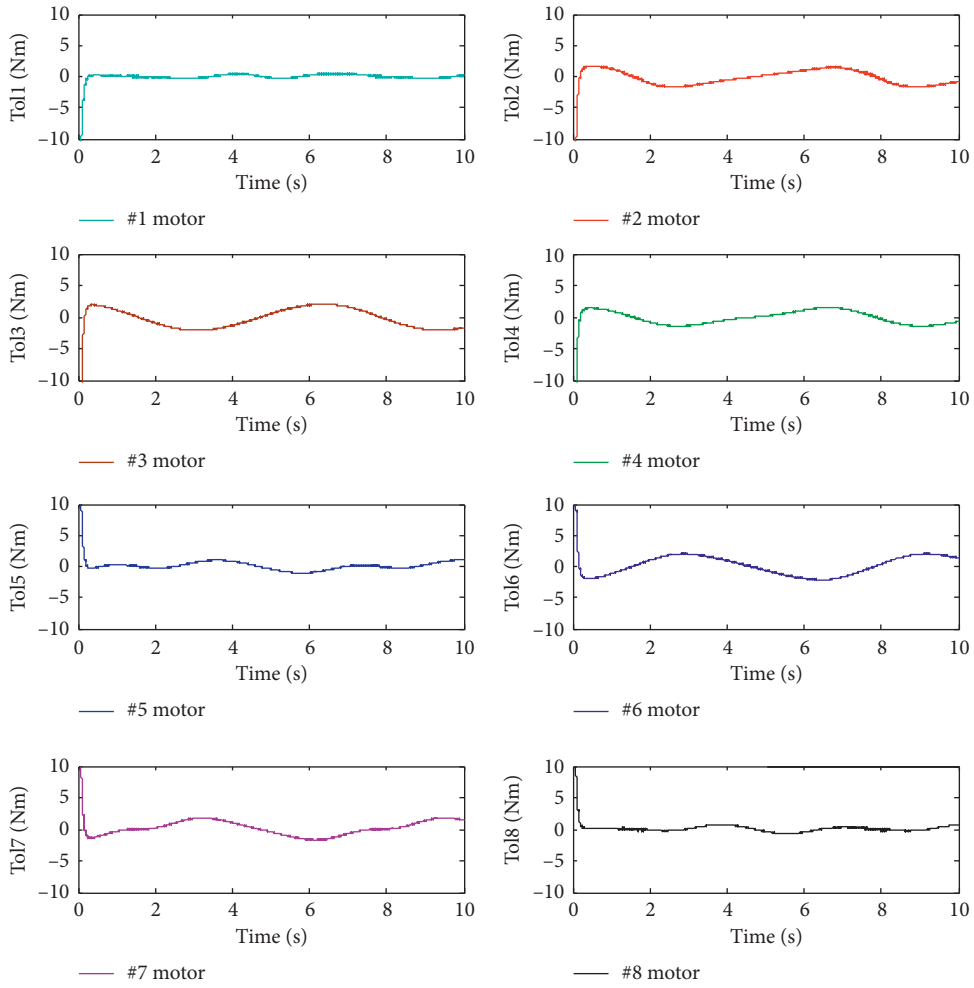

Figure 9: Control input of motors.

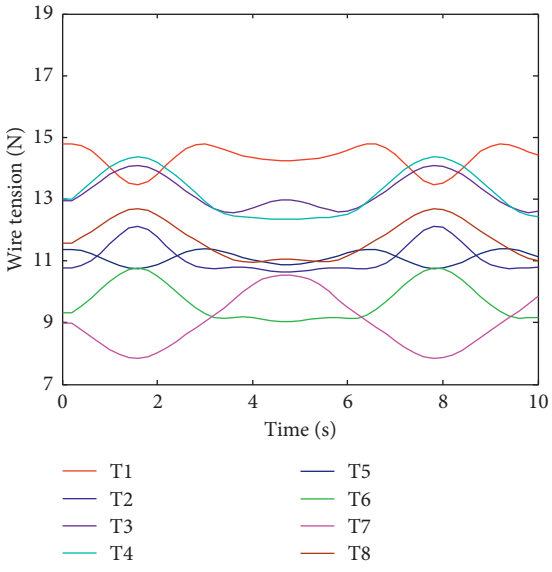

Figure 10: Wire tension.

library MFC to design the visual interface of the program. The software interface of WDPR prototype experiment mechanism is designed by class library MFC.

In the control process, the Jacobian matrix $\mathbf{J}$ and its pseudoinverse matrix $\mathbf{J}^{+}$ involve a lot of matrix operations, and the calculation speed is too slow to realize real-time online computation. Therefore, through MATLAB simulation, the Jacobian matrix $\mathbf{J}$ and its pseudoinverse matrix $\mathbf{J}^{+}$ are calculated offline and invoked in real-time during the control to improve the control efficiency of the WDPR prototype mechanism. The performance of the existing hardware devices cannot meet the requirements of complex motion experiments. Therefore, the feasibility and control property of the proposed control law is verified through a single DOF motion experiment. The theoretical pose of the end-effector is set as follows: $X_d = [\,0 \;\; 0 \;\; -0.582 \;\; 0 \;\; (\mathrm{pi}/6) \times \sin(\mathrm{t}) \;\; 0\,]^{\mathrm{T}}$. The experimental results of the WDPR prototype are shown in Figures 13–17.

In Figures 13 and 14, the experimental results show that the experimental pose curves of the end-effector are

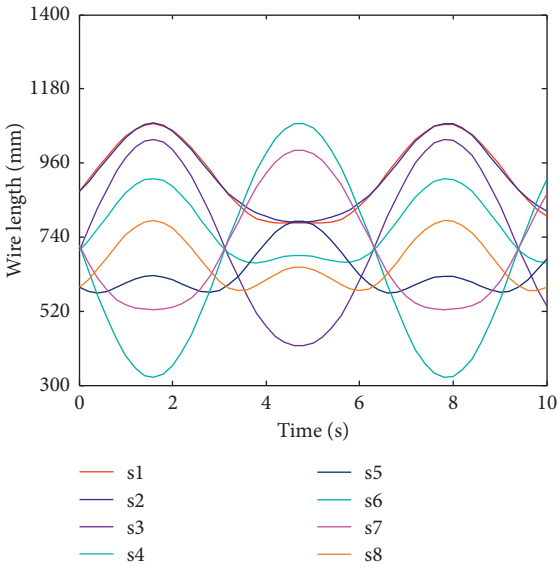

Figure 11: Wire length.

Figure 12: IMAC controller.

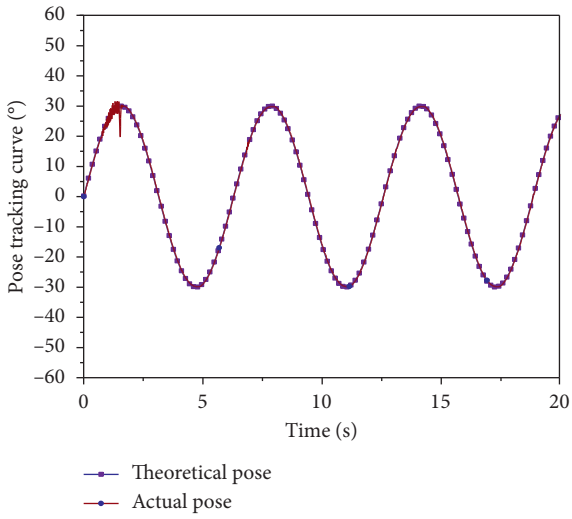

Figure 13: Pose tracking curve.

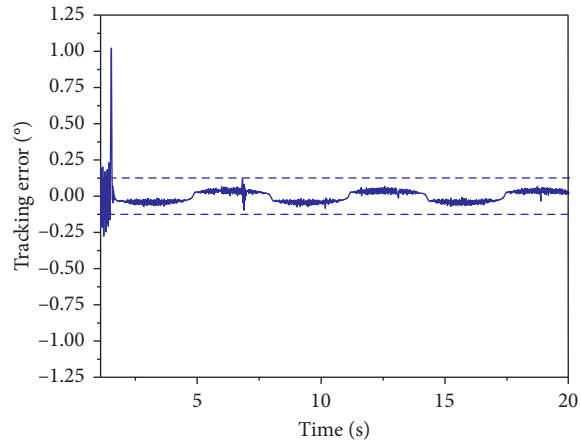

Figure 14: Pose tracking error curve.

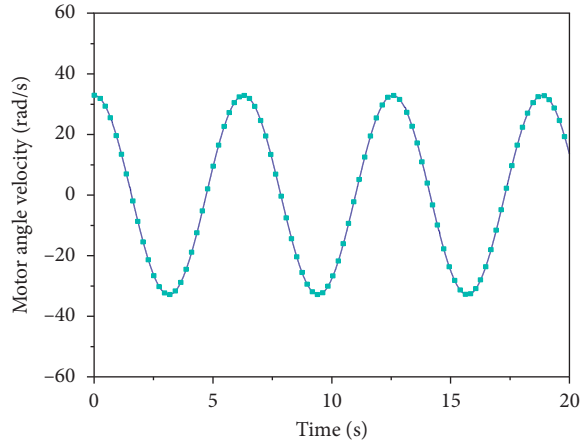

Figure 15: Actual angular velocity of #1 motor.

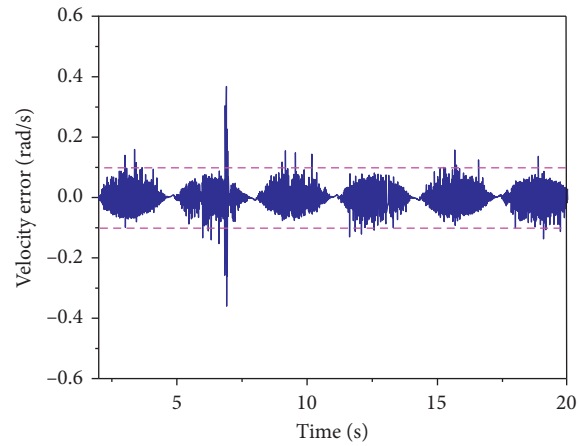

Figure 16: Absolute error of #1 motor (angular velocity).

smooth and continuous. And the error between the theoretical pose and the experimental pose is about ±0.05°. Taking #1 motor as an example, it can be seen from Figures 15 and 16 that the trend of the actual angular velocity of #1 motor is correct and the absolute error of #1 motor is ±0.1 rad/s. And it can be seen from Figure 17 that the actual output torque of #1 motor is within the range of rated torque (1.27 Nm). The above experimental results are satisfactory. Therefore, it can be concluded that the proposed backstepping sliding mode robust control is correct and effective, and it can be used on the prototype for the wind tunnel test.

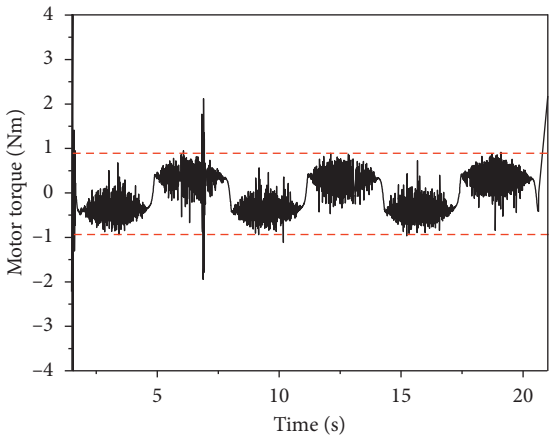

Figure 17: Output torque of #1 motor.

7. Conclusions

In this study, the dynamic model for WDPR used in the wind tunnel test is constructed. According to its dynamic model, a backstepping sliding mode robust control is designed based on a nonlinear disturbance observer. Through using the designed nonlinear disturbance observer, the equivalent disturbance is observed. And the equivalent compensation is introduced into the designed backstepping sliding mode robust control, which achieves complete suppression of the disturbance. The Lyapunov second method is used to prove the correctness of the designed control strategy and analyze the stability of the closed-loop system. The simulation results show that the robust control strategy has high control precision, and the designed control scheme is feasible. Finally, the effectiveness of the proposed control scheme is further proved through prototype experiment. The designed backstepping sliding mode robust control has certain innovation, guidance, and practicality for the application of WDPR prototype in the wind tunnel test. The future research direction is to improve the hardware performance of WDPR and carry out composite motion and six degree of freedom motion experiments on the prototype to further verify the feasibility of the designed control law.

Data Availability

The data used to support the findings of this study are available from the corresponding author upon request.

Conflicts of Interest

The authors declare that they have no conflicts of interest.

Acknowledgments

This study was supported by the Scientific Research Foundation of Nanjing Institute of Technology (nos. YKJ201917 and CKJA201903) and the National Natural Science Foundation of China (no. 11472234).

References

[1] Q. Chen, W. Chen, G. Yang, and R. Liu, "An integrated two-level self-calibration method for a cable-driven humanoid arm," *IEEE Transactions on Automation Science and Engineering*, vol. 10, no. 6, pp. 380–391, 2013.

[2] B. Zi, J. Cao, H. Zhu, and H. Sun, "Comparative study of cable parallel manipulators with and without hybrid-driven planar five-bar mechanism," *Applied Mathematical Modelling*, vol. 38, no. 24, pp. 5994–6017, 2014.

[3] H. Yuan, E. Courteille, M. Gouttefarde, and P.-E. Hervé, "Vibration analysis of cable-driven parallel robots based on the dynamic stiffness matrix method," *Journal of Sound and Vibration*, vol. 394, pp. 527–544, 2017.

[4] B. Gao, Z. Zhu, J. Zhao, and L. Jiang, "Inverse kinematics and workspace analysis of a 3 DOF flexible parallel humanoid neck robot," *Journal of Intelligent & Robotic Systems*, vol. 87, no. 2, pp. 211–229, 2017.

[5] A. Aflakian, A. Safaryazdi, M. Tale Masouleh, and A. Kalhor, "Experimental study on the kinematic control of a cable suspended parallel robot for object tracking purpose," *Mechatronics*, vol. 50, pp. 160–176, 2018.

[6] J.-M. Heo, B.-J. Park, J.-O. Park, C.-S. Kim, J. Jung, and K.-S. Park, "Workspace and stability analysis of a 6-DOF cable-driven parallel robot using frequency-based variable constraints," *Journal of Mechanical Science and Technology*, vol. 32, no. 3, pp. 1345–1356, 2018.

[7] X. Liu, Y. Qiu, and Y. Sheng, "Stiffness enhancement and motion control of a 6-DOF wire-driven parallel manipulator with redundant actuations for wind tunnels," *Acta Aeronautica Et Astronautica Sinica*, vol. 30, no. 6, pp. 1156–1164, 2009.

[8] M. A. Khosravi and H. D. Taghirad, "Robust PID control of fully-constrained cable driven parallel robots," *Mechatronics*, vol. 24, no. 2, pp. 87–97, 2014.

[9] R. Babaghasabha, M. A. Khosravi, and H. D. Taghirad, "Adaptive robust control of fully-constrained cable driven parallel robots," *Mechatronics*, vol. 25, pp. 27–36, 2015.

[10] W. Kraus, P. Miermeister, V. Schmidt, and A. Pott, "Hybrid position-force control of a cable-driven parallel robot with experimental evaluation," *Mechanical Sciences*, vol. 6, no. 2, pp. 119–125, 2015.

[11] T. Wang, S. Tong, J. Yi, and H. Li, "Adaptive inverse control of cable-driven parallel system based on type-2 fuzzy logic systems," *IEEE Transactions on Fuzzy Systems*, vol. 23, no. 5, pp. 1803–1816, 2015.

[12] R. Babaghasabha, M. A. Khosravi, and H. D. Taghirad, "Adaptive robust control of fully constrained cable robots: singular perturbation approach," *Nonlinear Dynamics*, vol. 85, no. 1, pp. 607–620, 2016.

[13] H. Jabbari Asl and J. Yoon, "Robust trajectory tracking control of cable-driven parallel robots," *Nonlinear Dynamics*, vol. 89, no. 4, pp. 2769–2784, 2017.

[14] L. Pascal, L. Michel, and R. Claude, "Design of a parallel wire driven manipulator for wind tunnels," in *Proceedings of the Workshop on Fundamental Issues and Future Research Directions for Parallel Mechanism and Manipulators*, pp. 187–194, Berlin, Germany, 2002.

[15] X. Liu, Y. Zheng, and L. Qi, "Overview of wired-driven parallel kinematic manipulators for aircraft wind tunnels," *Acta Aeronautica Et Astronautica Sinica*, vol. 25, no. 4, pp. 393–400, 2004.

[16] M. Pu, Q. Wu, C. Jiang et al., "New fast terminal sliding mode and its application to near space vehicles," *Acta Aeronautica Et Astronaut Ica Sinica*, vol. 32, no. 7, pp. 1283–1291, 2011.
[17] W. H. Chen, D. J. Balance, P. J. Gawthrop, and J. O. Reilly, "A nonlinear disturbance observer for robotic manipulator," *IEEE Transactions on Industrial Electronics*, vol. 47, no. 4, pp. 932–938, 2000.
[18] Q. Ai, C. Zhu, J. Zuo, W. Meng, Q. Liu, and Q. Sheng, "Xie and ming yang, "disturbance-estimated adaptive backstepping sliding mode control of a pneumatic muscles-driven ankle rehabilitation robot"," *Sensors*, vol. 18, no. 1, pp. 1–21, 2018.
[19] D. X. Ba, T. Q. Dinh, and K. K. Ahn, "An integrated intelligent nonlinear control method for a pneumatic artificial muscle," *IEEE/ASME Transactions on Mechatronics*, vol. 21, no. 4, pp. 1835–1845, 2016.
[20] W. Chen, S. S. Ge, J. Wu, and M. Gong, "Globally stable adaptive backstepping neural network control for uncertain strict-feedback systems with tracking accuracy known a priori," *IEEE Transactions on Neural Networks and Learning Systems*, vol. 26, no. 9, pp. 1842–1854, 2015.
[21] B. Chen, H. Zhang, and C. Lin, "Observer-based adaptive neural network control for nonlinear systems in nonstrict-feedback form," *IEEE Transactions on Neural Networks and Learning Systems*, vol. 27, no. 1, pp. 89–98, 2016.
[22] H. Wang, B. Chen, C. Lin, and Y. Sun, "Observer-based neural adaptive control for a class of MIMO delayed nonlinear systems with input nonlinearities," *Neurocomputing*, vol. 275, pp. 1988–1997, 2018.
[23] C.-W. Kuo and C.-C. Tsai, "Quaternion-based adaptive backstepping RFWNN control of quadrotors subject to model uncertainties and disturbances," *International Journal of Fuzzy Systems*, vol. 20, no. 6, pp. 1745–1755, 2018.